ORNL/SUB/83-51926/1

MILLIMETER WAVE DIELECTRIC PROPERTY MEASUREMENT OF GYROTRON WINDOW MATERIALS

TECHNICAL REPORT FOR THE PERIOD January 26, 1983 through February 29, 1984 (Rockwell Report No. SC5357.2TR)

FED LIBRARY FEB 1 1985

W.W. HO

APRIL 1984

FUSION ENERGY DIVISION LIBRARY

Report prepared by

ROCKWELL INTERNATIONAL SCIENCE CENTER
1049 Camino Dos Rios
Thousand Oaks, CA 91360

Under

Subcontract Purchase Order No. 11Y-51926C

For

OAK RIDGE NATIONAL LABORATORY
Oak Ridge, Tennessee 37831

Operated by

MARTIN MARIETTA ENERGY SYSTEMS, INC.
for the
U.S. DEPARTMENT OF ENERGY
Under Contract No. DE-AC05-840R21400

Rockwell International
Science Center

SC5357.2TR

TABLE OF CONTENTS

		Page
1.0	ABSTRACT	1
2.0	SUMMARY	2
3.0	EXPERIMENTAL METHOD	5
	3.1 Free-Space Transmission and Reflection Method	5
	3.2 Resonant Cavity Perturbation Method	8
	3.3 Chemical and Microstructural Analysis	8
4.0	EXPERIMENTAL RESULTS	9
	4.1 Alumina	9
	4.2 Single Crystal Sapphire	36
	4.3 Other Ceramics	36
	4.4 Fluorocarbon Fluids	43
5.0	CONCLUSIONS AND RECOMMENDATIONS	45

OAK RIDGE NATIONAL LABORATORY LIBRARY
3 4456 0027699 3

LIST OF FIGURES

Figure		Page
1	Measured loss tangents for ceramic Al_2O_3 at room temperature as a function of frequency	10
2	Measured change in dielectric constant as a function of temperature for Coors AD-995 alumina at 35 GHz	13
3	Measured loss tangent as a function of temperature for Coors AD-995 alumina	14
4	Photograph taking by scanning electron microscope for Wesgo AL-995 alumina sample showing a significant presence of voids	16
5	Photograph taken by scanning electron microscope for Coors AD-995 alumina. The presence of voids are less in both number density and size when compared to the results obtained for Wesgo AL-995 sample	16
6	Photograph taken by scanning electron microscope for Coors AD-999 alumina sample	17
7	Photograph taken by scanning electron microscope for Union Carbide hot-pressed alumina sample, (Al_2O_3-CR-10-18)	17
8	SEM photographs of all four samples studied taken under identical magnifications for direct comparison purposes	18
9	SEM photographs of Union Carbide alumina sample showing the presence of large grains	20
10	Microprobe chemical analysis by EDAX for Union Carbide hot-presses alumina (Al_2O_3-CR-10-18) taken near center of sample for a fractured surface. The gold peaks are from the coating and not from the sample. No other minor impurities are observed	20
11	Microprobe chemical analysis by EDAX for Union Carbide hot-pressed alumina (Al_2O_3-CR-10-18) taken near outer edge of sample for a fractured surface under identical experimental conditions as previous case. In addition to the Al and Au peaks, significant levels of Na, Si, Cl, K, and Ca are detected	21

LIST OF FIGURES

Figure		Page
12	Microprobe chemical analysis by EDAX for Union carbide hot-pressed alumina (Al_2O_3-CR-10-18) taken near center of sample on a polished surface. The instrument sensitivity and integration time are identical with the two previous spectra. Comparison with the results obtained for the fractured surface indicated that polishing did not introduce significant contamination of the surface	21
13	Scanning transmission electron micrograph of typical intergranular structure for Wesgo AL-995 alumina showing the presence of glassy phase	23
14	Scanning transmission electron micrograph of typical intergranular structure for Coors AD-995 (batch 8360, firing No. L58-150) alumina showing the presence of glassy phase	24
15	Scanning transmission electron micrograph of Coors AD-999 alumina sample. Large particles with beta alumina-like structures are present	25
16	Scanning transmission electron micrograph of Union Carbide hot-pressed alumina sample (Al_2O_3-CR-10-18), showing the absence of any detectable glassy phase	26
17	Powder x-ray diffraction pattern of Wesgo AL-995 alumina sample showing presence of silica, spinel, and calcium aluminate as crystalline secondary phases	27
18	Powder x-ray diffraction pattern of Coors AD-995 alumina sample. The concentrations of silica, spinel and calcium aluminate are lower by comparison to the Wesgo AL-995 material	28
19	Powder x-ray diffraction pattern of Coors AD-999 alumina sample. The concentrations of silica and calcium aluminate secondary crystalline phases are much higher, but there is no evidence for the presence of spinel	29
20	Powder x-ray diffraction pattern of Union Carbide hot-pressed alumina sample, showing no peaks associated with spinel or calcium aluminate and low concentration of silica	30

LIST OF FIGURES

Figure		Page
21	X-ray diffraction pattern of alumina starting powder used in fabrication of Union Carbide sample. There is no evidence of any peak associated with crystalline phases other than Al_2O_3	31
22	SEM and EDAX data for crystalline spinel found in the Wesgo AL-995 material	32
23	SEM and EDAX data for crystalline calcium aluminate found in the Coors AD-995 material	33
24	Measured loss tangents as a function of temperature for GTE AY6 and PY6 sintered silicon nitride at 35 GHz	39

LIST OF TABLES

Table		Page
I	Alumina Data Summary: Room Temperature Dielectric Properties (23°C)	11
II	Temperature Dependence Studies of Dielectric Properties for Sintered Alumina	12
III	Single Crystal Aluminum Oxide (Sapphire) Data Summary	37
IV	Hot-pressed Ceramic Spinel ($MgOAl_2O_3$) and Aluminum Oxynitride (ALON) Data Summary	40
V	Sintered Silicon Nitride (Si_3N_4) Data Summary	41
VI	Room Temperature (23°C) Dielectric Properties at 35 GHz for Sintered Si_3N_4 (1% BeO) and for Hot-pressed Beryllium Oxide	42
VII	Fluorocarbon Fluid (Fluorinert) Data Summary	44

1.0 ABSTRACT

The objectives of this program are to determine the millimeter wave dielectric properties of various single crystal and ceramic materials and coolant fluids in order to assess their transmission properties for high power Gyrotron window applications. Chemical and microstructural analysis are carried out for identifying the key material parameters controlling the millimeter absorption in these materials in support of future advanced materials development efforts.

2.0 SUMMARY

This report presents the results obtained for the program, "Millimeter Wave Dielectric Property Measurements of Gyrotion Window Materials," Martin Marietta subcontract No. 12Y-51926C, covering the period of performance 01/26/83 through 02/29/84. The dielectric properties of various standard and advanced ceramics were characterized as a function of frequency over the range 30 GHz-110 GHz, and selected materials were studied at temperatures up to 1200°C. In addition, single crystal sapphire and several fluorocarbon fluids were also studied. These results are summarized in tabular and graphic format in Section 4.0 of this report. A materials characterization effort, aimed at basic understanding of the parameters and mechanisms controlling the observed dielectric loss in the best candidate window materials was initiated during the last quarter of the program. This effort included chemical and microstructural analysis for determining grain size distribution, porosity and the presence, location and chemical state of minor and trace elements within these materials. In addition to standard quantitative analysis methods, X-ray Diffraction (XRD), Scanning Electron Microscopy (SEM), Scanning Transmission Electron Microscopy (STEM), and Energy Dispersive X-ray Analysis (EDAX) are used to measure the physical and chemical properties of micro-crystalline and intergranular secondary and impurity phases.

The results obtained for the millimeter wave dielectric properties of the Al_2O_3 materials studied in this program indicated that, as expected, single crystal sapphire has the lowest loss tangent. The loss tangent for z-cut optical grade sapphire samples (Crystal Systems Hemlite) was found to be 2.5×10^{-4} at 90-100 GHz. The best ceramic alumina samples (Coors AD-995, Ampex 99.5%, Wesgo AL-995) have losses approximately 50% larger, while the fine-grained alumina samples (Coors AD-999, Union Carbide hot-pressed alumina) showed surprisingly high losses (factor of 5 to 10 larger) when compared to sapphire. The dielectric constants for all the Al_2O_3 materials studied are essentially independent of frequency over the range of measurements while the loss tangents decreased monotonically with decreasing frequency. The increase

in dielectric constant with temperature was found to be approximately linear over the range 25-1200°C while the loss showed a drastic increase at temperatures beyond 800°C. Preliminary chemical and microstructural analysis carried out on these ceramic samples yielded differences in trace element composition, grain structure, and secondary and intergranular phases. Establishment of the correlation of these material properties with the observed dielectric response is essential in order to provide the necessary information for developing advanced ceramic alumina materials with properties approaching those for sapphire. A systematic investigation is currently underway to identify the basic mechanisms and key material and processing parameters controlling the millimeter wave absorption in this class of material.

It is also not clear at present whether the measured loss in sapphire is intrinsic to the material or still dominated by trace impurities or crystal defects. Consequently, the ultimate achievable value for the millimeter wave absorption of alumina is not known. Dielectric measurements are planned on a series of well-characterized sapphire samples of different optical quality grades as a function of both frequency and temperature in order to establish the intrinsic millimeter wave dielectric response in single crystal sapphire.

Of the other candidate ceramic window materials examined, hot-pressed spinel was found to have loss tangents comparable to sapphire and better than the best alumina material. ALON and BeO have loss tangents comparable to alumina at 35 GHz but are substantially higher than alumina at 90-110 GHz. The various silicon nitride samples studied all showed loss tangents which are an order of magnitude larger than alumina and it is likely that extensive materials development need to be undertaken before they can be improved to be comparable to the other candidate window materials.

Three different types of fluorocarbon fluids were studied in the current program, (3M Fluorinert FC-43, FC-75 and FC-104). Their dielectric properties were determined at 8.36 GHz, 35 GHz, 60 GHz and 95 GHz. The results were very similar for FC-75 and FC-104, with loss tangent values of 0.008 at 8.35 GHz, decreasing to approximately 0.003 at 95 GHz. By contrast,

the fall-off in loss tangent with increasing frequency was substantially faster in FC-43, with values of 0.007 at 8.36 GHz and 0.001 at 95 GHz. Exposure of these fluids to liquid water did not significantly change their millimeter wave dielectric properties, nor did an increase in temperature from 23°C to 50°C.

3.0 EXPERIMENTAL METHOD

Two separate measurement methods were utilized for determining the millimeter wave dielectric properties of the samples studied. Laboratory capabilities for each of these approaches have been established at selected frequency intervals within the range 30-110 GHz. Standard free-space transmission and reflection bridges, utilizing either collimated or focused beams, are used to measure the dielectric properties of planar disk samples. For cases where large samples are not available and for liquids, a cavity perturbation approach, utilizing various right rectangular and cylindrical cavity resonators, is used. Brief descriptions of these two measurement methods are given in the following discussion.

3.1 Free-Space Transmission and Reflection Method

For this method, a plate of the sample material of uniform thickness is placed between a set of high directivity transmitter and receiver horns. The observables are the power transmission and reflection coefficients and/or their relative phase changes referenced to the incident power. In principle, measurements of any two of these four parameters will be sufficient for determining the dielectric constant and the loss tangent of the sample. In order to minimize diffraction effects, the planar dimensions of the sample must be made large compared to the free-space wavelength of the incident electromagnetic radiation and typical dimensions of the order of 10 λ or greater are generally required for very accurate measurements. At 35 GHz, samples with uniform thickness of the order of 9 cm on each side are necessary to meet this criterion. In addition, for very low loss materials, it is desirable to have as large a sample thickness as practical so that the attenuation within the sample can be made sufficiently high to be measurable to the required degree of accuracy.

The power transmission and reflection coefficients ($|T|^2, |R|^2$) for a plane wave incident on a low loss dielectric sheet, ($\tan^2\delta \ll 1$), with the

electric field vector polarized perpendicular to the plane of incidence can be well approximated by the following expressions:

$$|T|^2 = \frac{A^2(1 - a^2)^2 + 4A^2a^2 \sin^2\chi}{(1 - A^2a^2)^2 + 4A^2a^2 \sin^2 (\phi + \chi)} \tag{1}$$

$$|R|^2 = \frac{a^2(1 - A^2)^2 + 4A^2a^2 \sin^2\phi}{(1 - A^2a^2)^2 + 4A^2a^2 \sin^2 (\phi + \chi)} \tag{2}$$

$$A^2 = e^{-(2\pi dk \tan\delta)/\lambda_0(k - \sin^2\theta)^{1/2}} \tag{3}$$

$$\phi = (2\pi d/\lambda_0)(k - \sin^2\theta)^{1/2} \ , \ \chi = \tan^{-1}[(k/k-1)(k - \sin^2\theta)^{-1/2} \cos\theta \tan\delta] \tag{4}$$

$$a = \frac{[(k - \sin^2\theta)/\cos^2\theta]^{1/2} - 1}{[(k - \sin^2\theta)/\cos^2\theta]^{1/2} + 1} \tag{5}$$

where θ is the angle of incidence, k and $\tan\delta$ are the dielectric constant and the loss tangent of the sheet, λ_0 is the free-space wavelength of the incident radiation, and d is the thickness of the sheet.

The angle χ is the phase shift caused by the dielectric loss of the material and is only at most of the order of 2 degrees for k = 3 and $\tan\delta$ = 0.05 at all angles of incidence. Consequently, it can be neglected for most applications.

Although the two simultaneous transcendental equations given by (1) and (2) can be used to determine k and $\tan\delta$ at any arbitrary angle of incidence, it is more convenient to adopt an alternative procedure where the factor $(\phi + \chi)$

can be determined directly. This can be accomplished by either fixing the angle θ and varying the wavelength until the transmitted power is a maximum (or when the reflected power is a minimum), or alternatively, fixing the wavelength and varying the angle of incidence until the same conditions are observed. For these cases, the factor $(\phi + \chi)$ is equal to $N\pi$ where N is an integer including zero. An iterative procedure can then be used by first assuming $\tan\delta = 0$ and compute an initial value for k via Eq. (4). This preliminary value then can be substituted into either Eq. (1) or (2) to calculate $\tan\delta$, which can then be used to find a more accurate k, and so on. Convergence is sufficiently rapid for most cases so that one such iteration is usually sufficient to obtain final values of k and $\tan\delta$ which are consistent with the accuracy of he measurements.

The majority of the plate samples studied in the program are sufficiently thick, so that many reflection and transmission minima and maxima are present over each of the frequency bands, 33-50 GHz, 50-60 GHz, and 90-110 GHz. Consequently, the observed frequencies of these extrema, as well as the frequency interval between them, can be used to compute the dielectric constant of the sample. In addition, the loss tangents are low enough to allow independent determinations of k and $\tan\delta$ from the measurements of frequency and transmitted power respectively, without having to resort to the iterative procedure previously outlined. Under these conditions, k and $\tan\delta$ can be computed directly from the magnitude of the transmission coefficient and the frequency corresponding to the observed transmission maxima (or reflection minima), f_N, by the following expressions:

$$k = (c/2d\Delta f_N)^2 + \sin^2\theta \quad ;$$

$$k = (Nc/2df_N)^2 + \sin^2\theta \quad ;$$

$$\tan\delta = -\ln(A_N)[2(k - \sin^2\theta)/N\pi k] \quad ;$$

$$A_N = (1/2)\left\{[(1 - a^2)^2/a^4|T|^2 + 4/a^2]^{1/2} - (1 - a^2)/a^2|T|\right\} \quad ;$$

$$\Delta f_N = f_{(N+1)} - f_N \quad .$$

3.2 Resonant Cavity Perturbation Method

The basic experimental system for this approach consists of a fixed-frequency cavity resonator into which a small sample of regular geometry is inserted. The dielectric constant and loss tangent of the sample are respectively computed from the observed shift in resonant frequency and the change in quality factor, Q, of the cavity. Various right cylindrical and right rectangular reflection type cavity resonators operating at frequencies of 8.4 GHz, 35 GHz, 60 GHz and 95 GHz are used in the current study for determining the dielectric properties of small rod-shaped ceramic samples and of the liquids.

This experimental method has been described in detail in a previous report, ("High Temperature Millimeter Wave Characterization of the Dielectric Properties of Advanced Window Materials," final report AMMRC TR 82-28, Contract No. DAAG46-79--007, Army Materials and Mechanics Research Center, May, 1982).

3.3 Chemical and Microstructural Analysis

In order to identify possible mechanisms giving rise to high dielectric losses in the materials studied, chemical and microstructural analysis are carried out to determine the presence and location of minor and trace elements and their chemical states within the material. In addition to standard quantitative analysis methods, x-ray diffraction (XRD), scanning electron microscopy (SEM), scanning transmission electron microscopy (STEM), and energy dispersive x-ray analysis (EDAX) are used on select ceramic samples to characterize the micro-crystalline and intergranular properties of secondary and impurity phases.

4.0 EXPERIMENTAL RESULTS

4.1 Alumina

The measured room temperature millimeter wave dielectric properties of the alumina samples are summarized in Table I. In addition to samples from commercial sources (Coors, Wesgo, Ampex), an Union Carbide hot-pressed sample was also studied. In general, the observed dielectric constants decreases slightly with increasing frequency, while the loss tangents are significantly larger at the higher frequencies. Where more than one sample of a particular type of material was available, good agreement was obtained for the loss tangents to within the stated measurement accuracy. The Coors AD-995 and Ampex 99.5% samples are vitually identical in terms of loss tangent values, while the Wesgo AL-995 sample was somewhat higher. By contrast, the Coors AD-999 and the Union Carbide hot-pressed samples showed surprising high loss. The frequency dependence of the loss tangents at room temperature for the low-loss materials (Coors AD-995, Ampex, Wesgo AL-995) are shown in Fig. 1., where the 3.5 GHz values reported by Westphal and Sils, ("Dielectric Constant and Loss Data," Technical Report AFML-TR-72-39, April 1972), are also shown. Except for a differece in magnitude, the general frequency behavior is very similar for all three cases.

The temperature dependences for the dielectric properties of Coors AD-995 at 35 GHz are summarized in Table II. The observed increase in both the dielectric constant and loss tangent are similar to those reported by Westphal and Sils at 3.5 GHz, (Figs. 2 and 3).

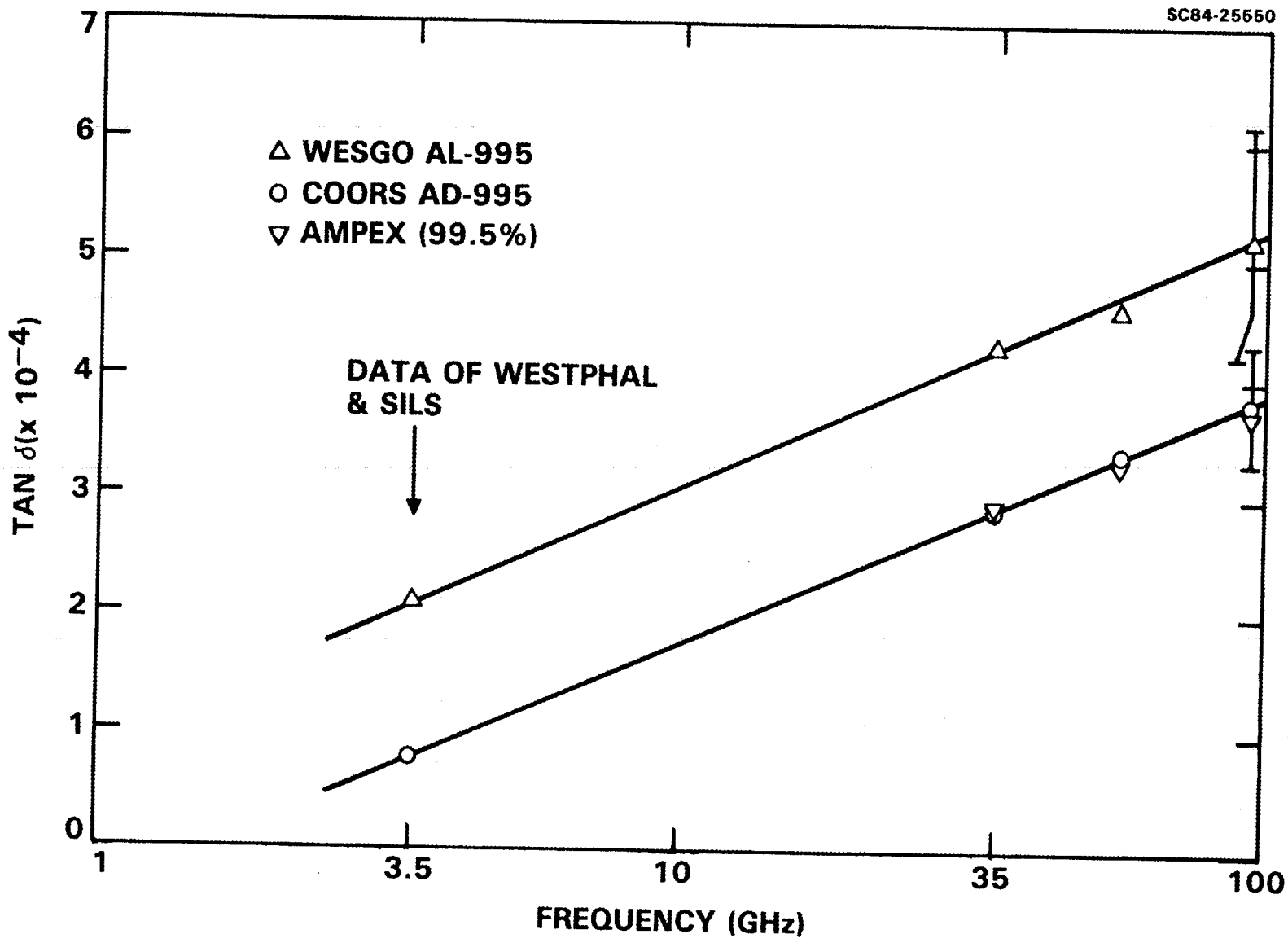

Fig. 1 Measured loss tangents for ceramic Al_2O_3 at room temperature as a function of frequency.

Table I

Alumina Data Summary:
Room Temperature Dielectric Properties (23°C)
(Sheet 1 of 2)

Sample Type: Coors AD-995 Sintered Alumina, Batch 8360, Firing No. L58-150

Sample Type: Coors AD-995 Sintered Alumina, Batch 8260, Firing No. L58-150								
			30-40 GHz		55-60 GHz		90-100 GHz	
Sample No.	Thickness (cm)	Density (gm/cc)	k (±0.008)	tanδ (x10^{-5}) (±10)	k ±0.010	tanδ (x10^{-5}) (±10)	k (±0.005)	tanδ (x10^{-5}) (±5)
1	3.8176	3.870	9.720	29	9.712	34	9.708	38
2	3.8176	3.873	9.730	29	9.718	34	9.714	38
3	3.8176	3.872	0.715	29	9.711	34	9.705	38
4	3.8176	3.871	9.724	29	9.715	34	9.709	38

Sample Type: Coors AD-995 and AD-999, Sintered Alumina, Thin Samples								
			30-40 GHz		55-60 GHz		90-100 GHz	
Sample No.	Thickness (cm)	Density (gm/cc)	k (±0.01	tanδ (x10^{-5})	k (±0.01)	tanδ (x10^{-5})	k (±0.01)	tanδ (x10^{-5}) (±20)
AD-995-1	0.7798	3.905	9.75	<40	9.74	<40	9.73	40
AD-995-2	0.7813	3.902	9.74	<40	9.73	<40	9.72	45
AD-995-3	0.6335	3.875	9.72	<40	9.71	<40	9.71	43
AD-999*	0.6368	3.882	9.71	100±40	9.71	120±40	9.71	133

Sample Type: Wesgo AL-995 Sintered Alumina								
			30-40 GHz		55-60 GHz		90-100 GHz	
Sample No.	Thickness (cm)	Density (gm/cc)	k	tanδ (x10^{-5})	k	tanδ (x10^{-5})	k	tanδ (x10^{-5})
1	5.0000	3.837	9.602 (±0.014)	43 (±10)	9.593 (±0.010)	46 (±12)	9.581 (±0.007)	52 (±10)
2 (Lot: 3006 Batch: 3175)	0.6491	3.845	9.61) (±0.01)	<40	9.60 (±0.01)	<40	9.58 (±0.01)	45 (±20)
3 (Lot: 3006 Batch: 3177)	0.6527	3.856	9.68 (±0.01)	<40	9.67 (±0.01)	<40	9.67 (±0.01)	50 (±20)

*Samples were also received where the measured densities were 3.934 gm/cc, but their dimensions (1.317 cm diameter, 0.324 cm thickness) were too small for the dielectric measurement requirements.

Table I

Alumina Data Summary:
Room Temperature Dielectric Properties (23°C)
(Sheet 2 of 2)

Sample Type: Union Carbide, Hot-pressed Alumina (Al_2O_3-CR-10-18)

Sample Diameter = 7.52 cm
Sample Thickness = 0.6528 cm
Sample Density = 3.863 gm/cc

Frequency	k	tanδ
30-40 GHz	9.495 ± 0.046	0.0030 ± 0.0005
55-60 GHz	9.501 ± 0.040	0.0033 ± 0.0008
90-100 GHz	9.512 ± 0.037	0.0036 ± 0.0015

Sample Type: Ampex 99.5% Sintered Alumina

			30-40 GHz		55-60 GHz		90-100 GHz	
Sample No.	Thickness (cm)	Density (gm/cc)	k (±0.008)	tanδ ($\times 10^{-5}$) (±10)	k ±0.010	tanδ ($\times 10^{-5}$) (±10)	k (±0.005)	tanδ ($\times 10^{-5}$) (±5)
1	2.9736	3.870	9.673	29	9.660	33	9.642	37
2	3.0858	3.870	9.669	31	9.662	34	9.635	38
3	2.9738	3.872	9.671	28	9.663	33	9.642	36
4	2.9721	3.875	9.680	31	9.670	32	9.654	36

Table II

Temperature Dependence of Dielectric Properties for
Sintered Alumina

Sample Material: Coors AD-995
Sample Shape: Thin rod, 0.0495 cm diameter
Measurement Method: Cavity perturbation
Frequency: 35 GHz

Temperature (°C)	k (±0.03)	tanδ ($\times 10^{-5}$) (±15)
23	9.72	32
470	10.24	50
750	10.59	81
915	11.00	99
1000	11.16	120
1110	11.49	145

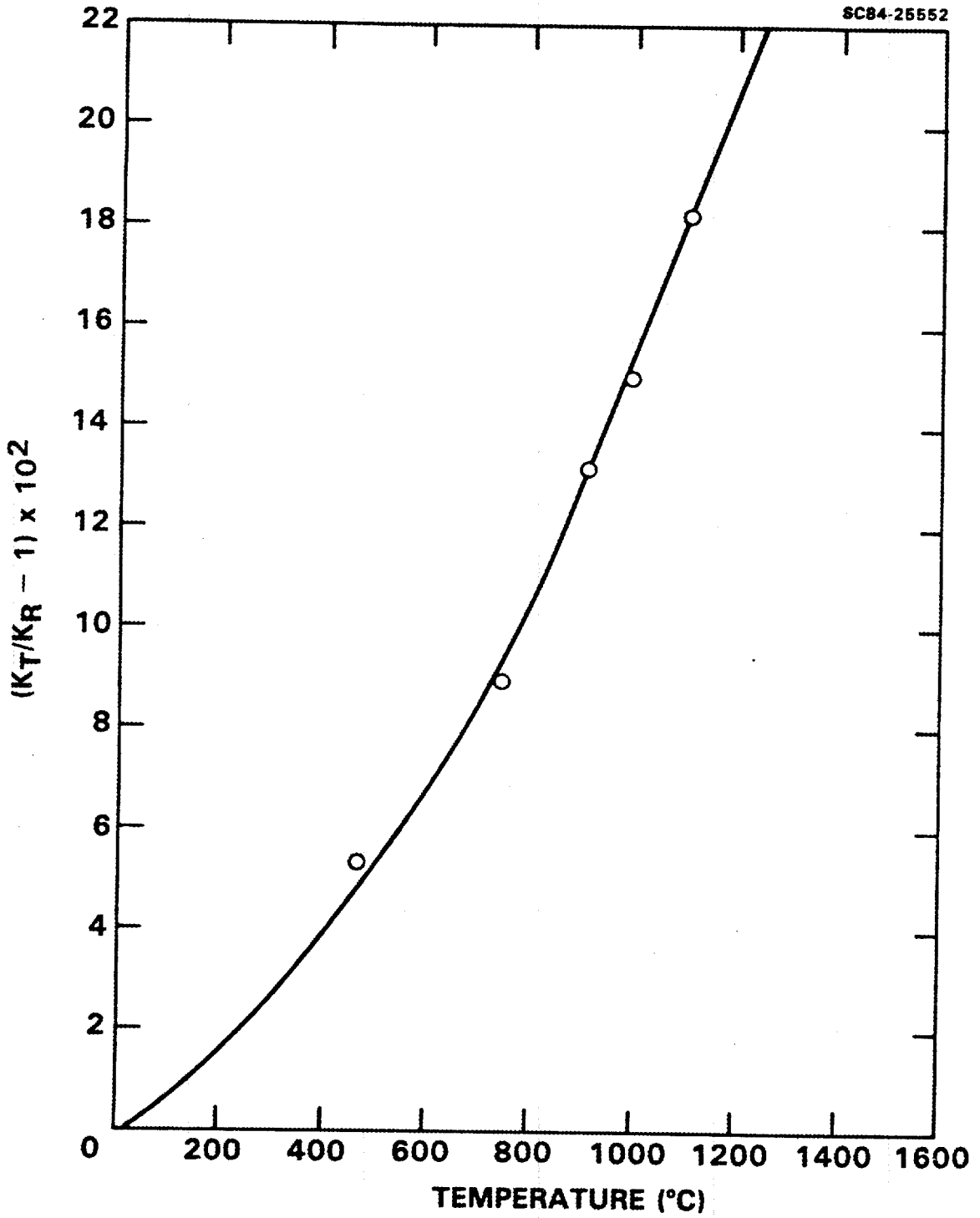

Fig. 2 Measured change in dielectric constant as function of temperature for Coors AD-995 alumina at 35 GHz.

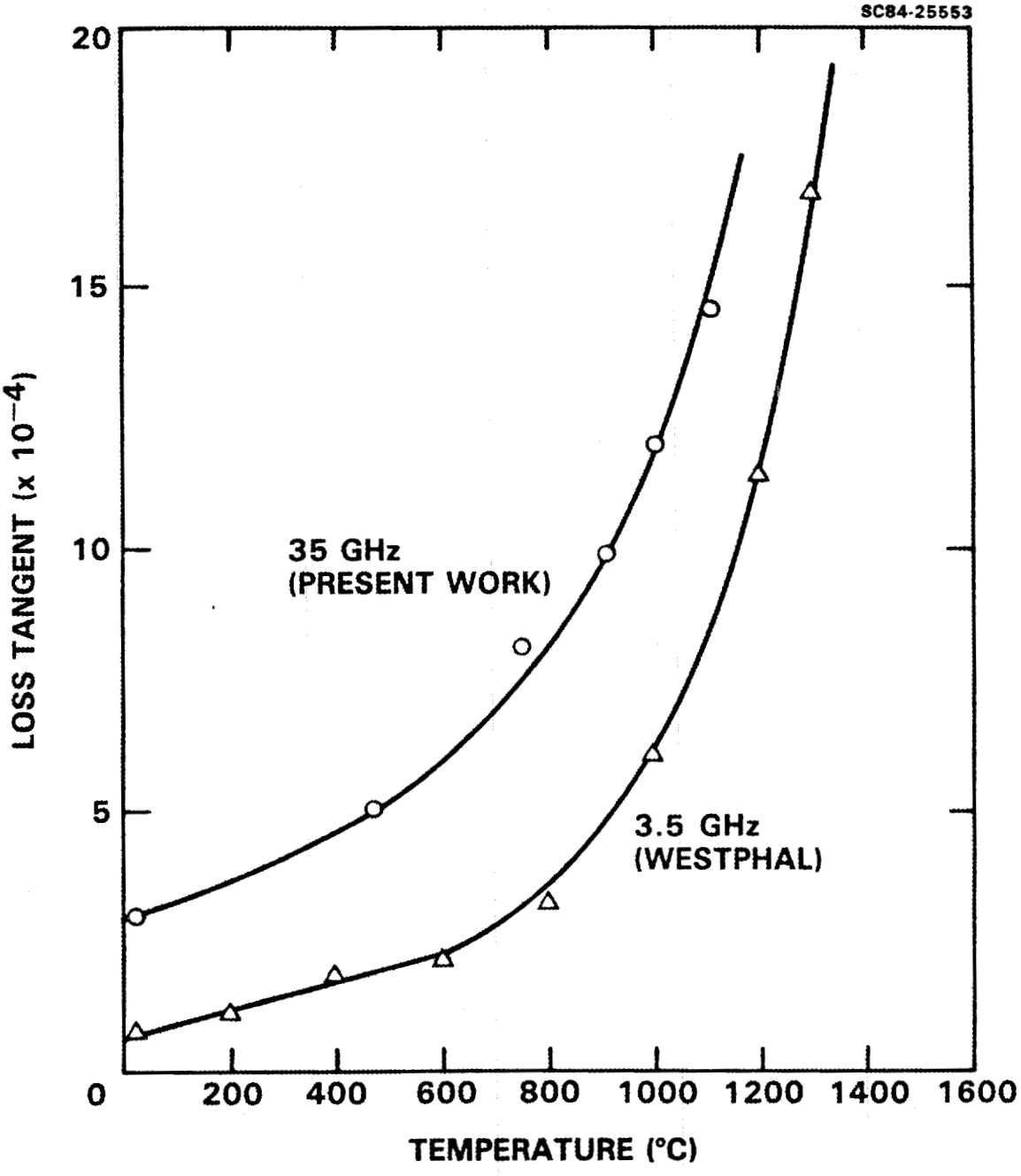

Fig. 3 Measured loss tangent as a function of temperature for Coors AD-995 alumina.

Chemical and microstructural analysis were carried out on the Coors AD-995, Coors AD-999, Wesgo AL-995, and the Union Carbide hot-pressed samples in an effort to correlate the observed dielectric properties with materials properties for identifying potential causes of the observed differences, (the Ampex samples were received too late for inclusion in this portion of the effort. Analysis are currently being carried out. We expect their properties to be similar to the Coors AD-995 material). SEM photographs of fracture surfaces for these samples are shown in Figs. 4-7. The grain structures for the Coors AD-995 and Wesgo AL-995 are very similar, consisting of smaller grains (5-10 μm) distributed in a much larger grain-size (~ 30 μm) matrix. Both samples showed the presence of voids, with the number density as well as average size being significantly smaller for the Coors AD-995 sample. This is most likely the reason for the observed lower density, and hence the lower dielectric constant, of the Wesgo AL-995 when compared to the Coors AD-995 sample. The Coors AD-999 and Union Carbide hot-pressed material are both fine-grained with no evidence of voids. Average grain size is of the order of 0.5-2.0 μm for Coors AD-999 and 2-4 μm for the Union Carbide material. For purposes of direct comparison, SEM photographs for all 4 samples taken at identical magnification are shown in Fig. 8, where the differences in microstructures are dramatically illustrated.

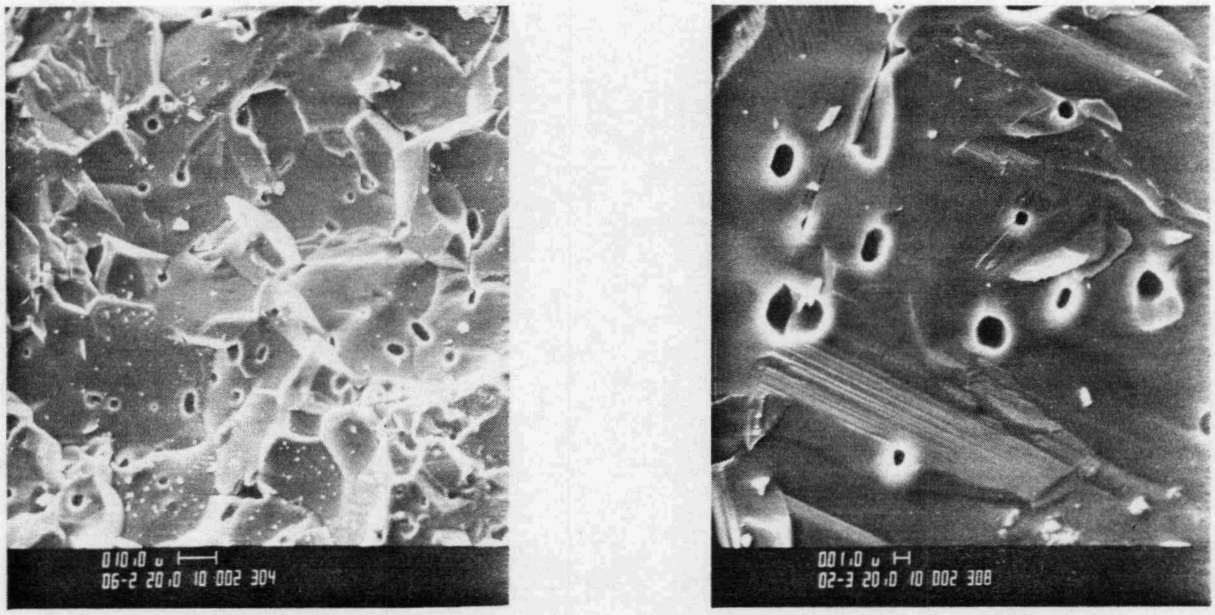

Fig. 4 Photograph taken by scanning electron microscope for Wesgo AL-995 alumina sample showing a significant presence of voids.

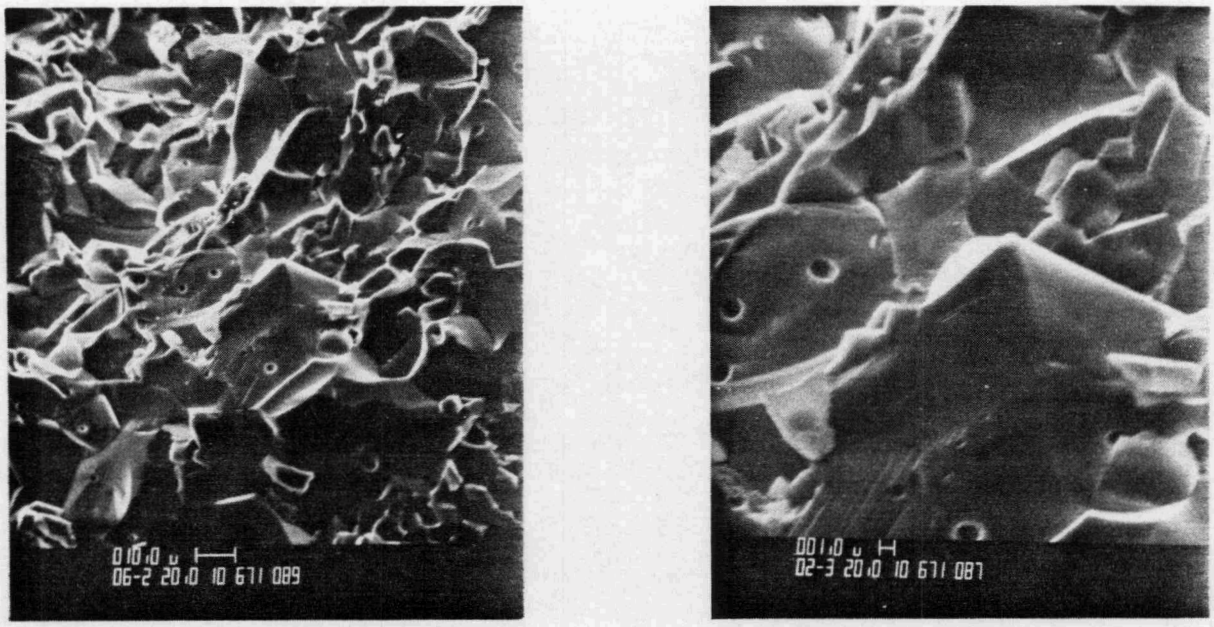

Fig. 5 Photograph taken by scanning electron microscope for Coors AD-995 alumina. The presence of voids are less in both number density and size when compared to the results obtained for Wesgo AL-995 sample.

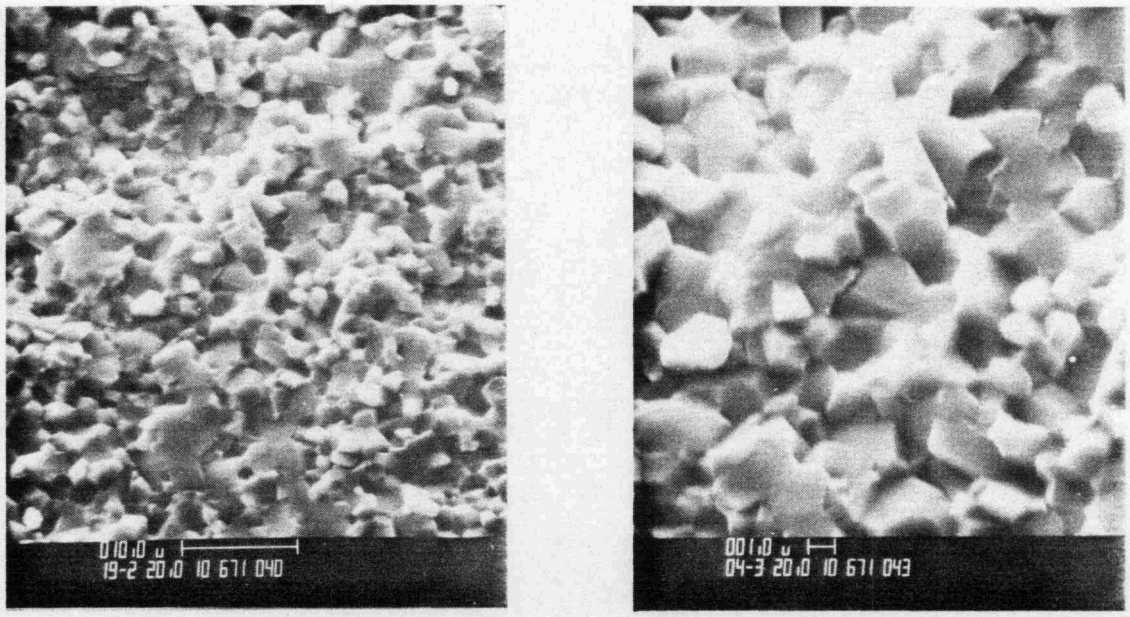

Fig. 6 Photograph taken by scanning electron microscope for Coors AD-999 alumina sample.

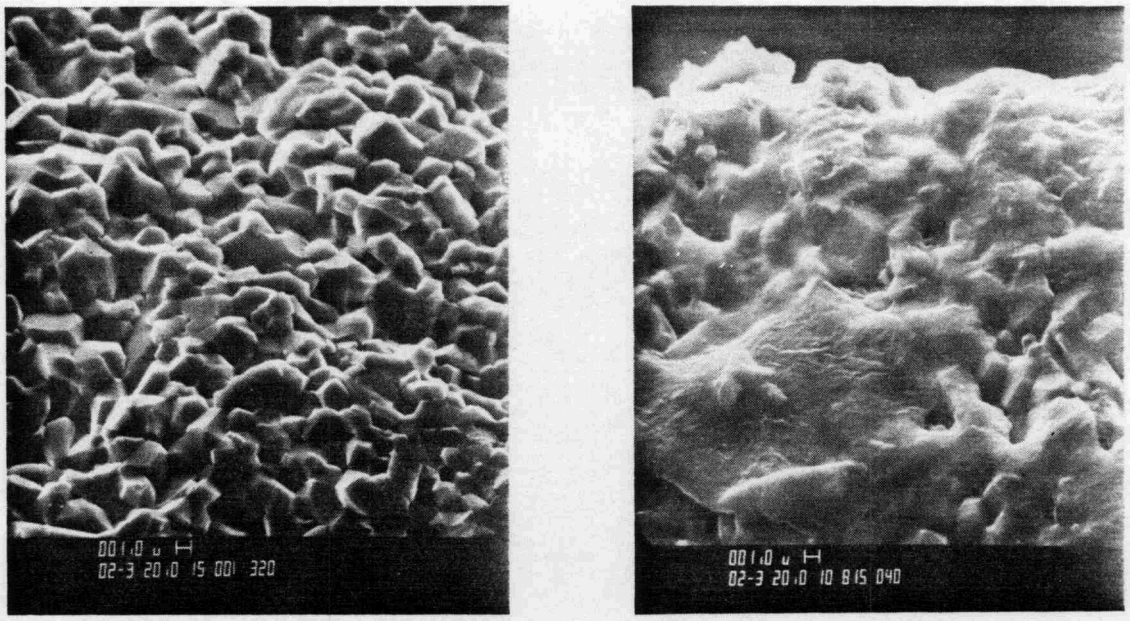

Fig. 7 Photograph taken by scanning electron microscope for Union Carbide hot-pressed alumina sample, (Al_2O_3-CR-10-18).

UNION CARBIDE Alumina

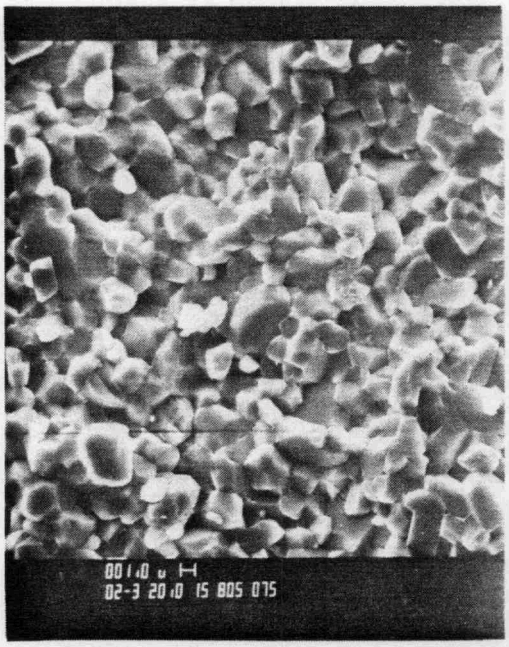

WESGO 995 Alumina

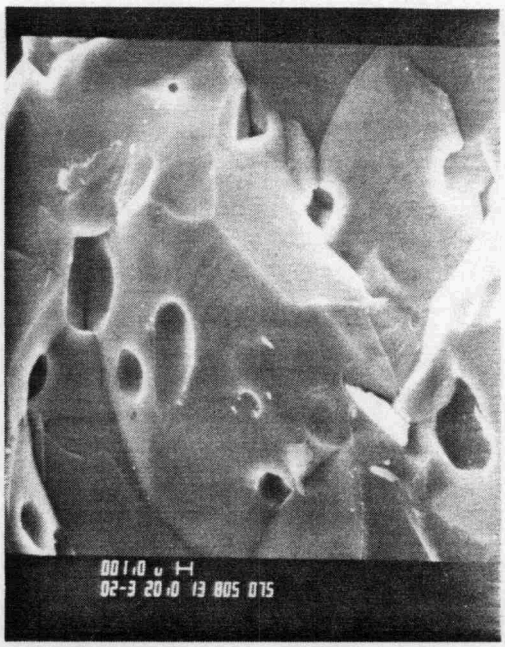

COORS 999 Alumina

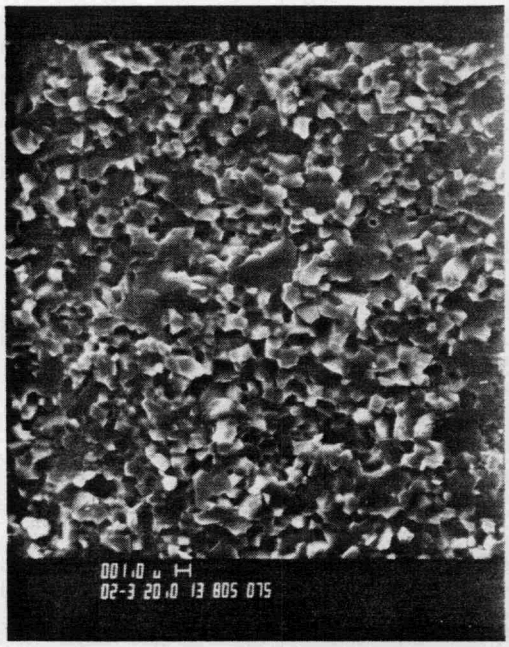

COORS 995 Alumina

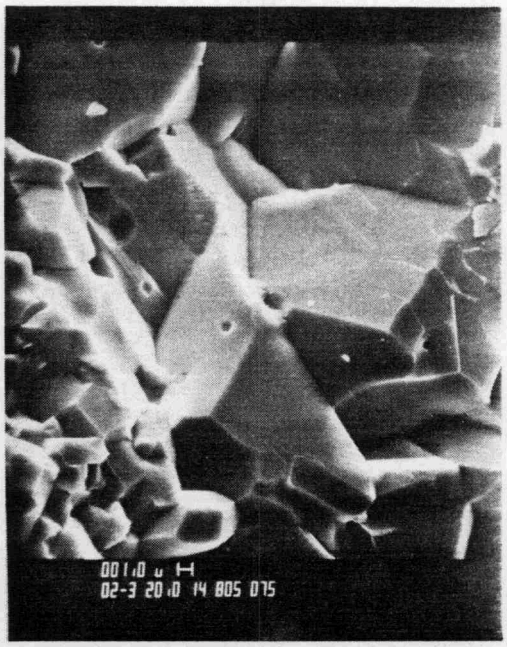

Fig. 8 SEM photographs of all four samples studied taken under identical magnifications for direct comparison purposes.

The Union Carbide material has occasional large grains (50-100 μm) which are fairly uniformly distributed throughout the sample. A typical region showing the presence of these large grains is illustrated in Fig. 9. In addition, as seen in Fig. 7, the structure for the Union Carbide material is significantly different in regions near the edge, or outer skin, of the sample. Although the presence of fine grains is still evident, there is an additional amorphous phase present which may possibly be one of the contributing factors to the observed dielectric properties. Microprobe chemical analysis by EDAX for this material also showed some interesting results. Figures 10-12 are EDAX spectra taken respectively for regions corresponding to those shown in Fig. 7 as well as for a polished surface in a region near the center of the sample. The polishing did not introduce any noticeable contamination, while the edge of the sample showed significant presence of other cations. In view of these results, further dielectric loss measurements were carried out by focusing down the incident microwave beam in an attempt to determine whether the loss tangent for this material is significantly different between the center of the sample and the edge of the sample near its outer skin. A spot size of approximately 2 cm in diamter was used at 35 GHz, and the transmitted power was measured as the spot was moved across the 7.5 cm diameter sample. The result obtained indicated that, indeed, the sample showed the least loss in the center, while the regions near the edge was approximately five times more lossy. The distribution of loss was axially symmetric and, to within the limit of spatial resolution, varied linearly with the distance from the center of the sample. The weighted average for the loss tangent over the entire surface of the sample was found to be in close agreement with the values given in Table I. Since chemical analysis carried out on the starting powder used in fabricating this hot-pressed sample indicated that it is extremely pure with very low levels of impurities, the evidences from the dielectric and SEM/EDAX measurements suggest that contamination is occurring at or near the outer surfaces of the sample due to the hot-pressing procedure.

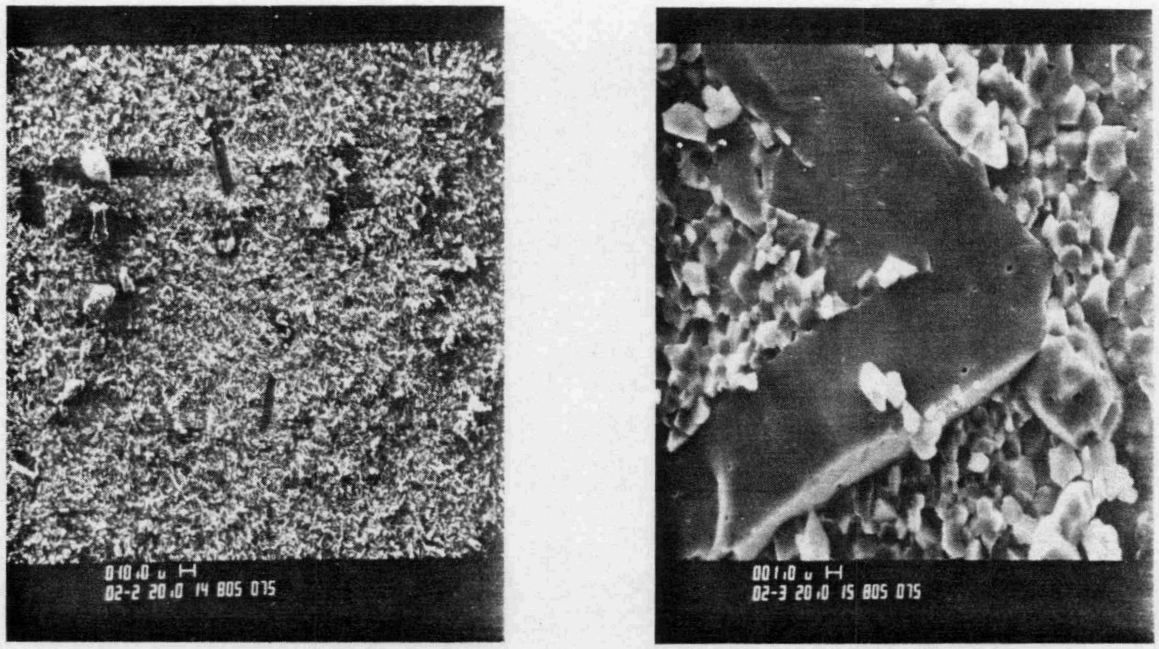

Fig. 9 SEM photographs of Union Carbide sample showing the presence of large grains.

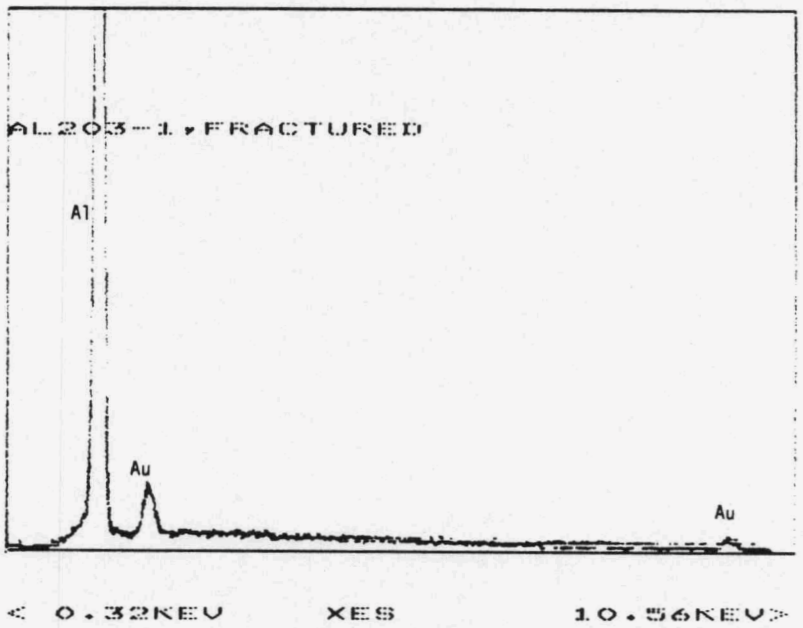

Fig. 10 Microprobe chemical analysis by EDAX for Union Carbide hot-presses alumina (Al_2O_3-CR-10-18) taken near center of sample for a fractured surface. The gold peaks are from the coating and not from the sample. No other minor impurities are observed.

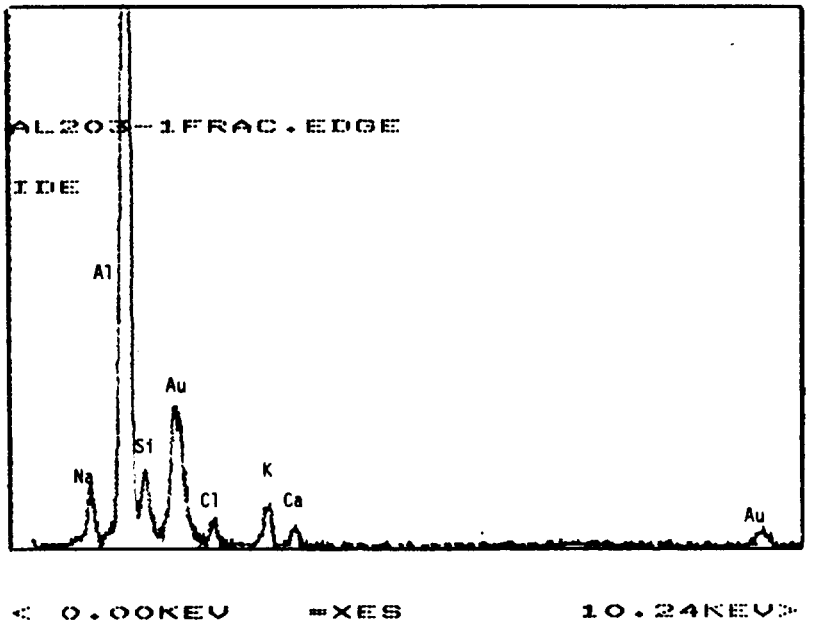

Fig. 11 Microprobe chemical analysis by EDAX for Union Carbide hot-pressed alumina (Al_2O_3-CR-10-18) taken near outer edge of sample for a fractured surface under identical experimental conditions as previous case. In addition to the Al and Au peaks, significant levels of Na, Si, Cl, K, and Ca are detected.

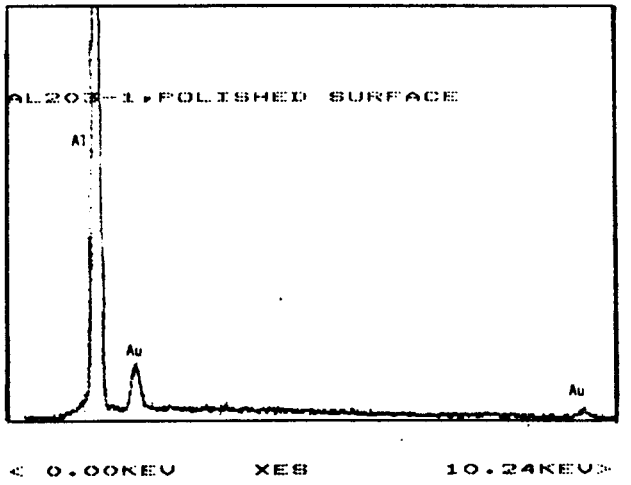

Fig. 12 Microprobe chemical analysis by EDAX for Union Carbide hot-pressed alumina (Al_2O_3-CR-10-18) taken near center of sample on a polished surface. The instrument sensitivity and integration time are identical with the two previous spectra. Comparison with the results obtained for the fractured surface indicated that polishing did not introduce significant contamination of the surface.

STEM analysis (Figs. 13-16) indicated that both the Coors AD-995 and Wesgo AL-995 materials have large pockets of glass at the grain junctions, while the Coors AD-999 and Union Carbide materials showed no evidence of a glassy phase. The glass pockets in the Coors AD-995 and Wesgo AL-995 samples contained Al, Ca, and traces of Fe in addition to Si, with the concentration for Ca and Fe being qualitatively slightly higher for the Wesgo material. The Coors AD-999 material contained large particles with beta alumina structure showing traces of K and possibly Pb. The Union Carbide material exhibited pores at the triple points with traces of Fe and Cr detected near some of the pores.

X-ray diffraction patterns taken on powders obtained by milling the alumina samples with an agate mortar and pestle are shown in Figs. 17-20 for the 4 different alumina materials. For comparison, the XRD pattern for the alumina starting powder used in preparation of the Union Carbide hot-pressed sample (CR-10-18) is shown in Fig. 21. The alumina starting powder showed no detectable levels of secondary crystalline phases, while the ceramic samples have XRD peaks corresponding to SiO_2, $MgAl_2O_4$ and $CaAl_2O_4$. This is expected since the Coors and Wesgo alumina use fluxes of either $CaOMgSiO_2$ or MgO in the sintering process, and silica is always present to some extent. A comparison of the Coors AD-995 results with those for the Wesgo AL-995 results showed that the concentration of crystalline SiO_2, $MgAl_2O_4$ and $CaAl_2O_4$ phases are all qualitatively lower in the Coors AD-995 sample. This trend is in agreement with the previously described STEM results of the calcium concentration in the intergranular glassy phase. A careful search by SEM and EDAX revealed the presence of micron-size spinel and calcium aluminate grains in both the Coors AD-995 and Wesgo Al-995 material, thus verifying the XRD findings. Typical results are given in Figs. 22 and 23 showing the presence of these secondary crystalline phases. The Coors AD-999 sample showed a higher concentration of silica and $CaAl_2O_4$ with no detectable spinel. This was very surprising since STEM analysis found no significant glass phase at the grain junctions or grain boundaries. Subsequent SEM analysis, however, did reveal localized regions in the sample where substantial silica were present. The most likely explanation for the apparent discrepancy between the STEM results and the XRD results for the Coors AD-999 material is that the material is inhomogeneous and the STEM analysis were carried out in regions

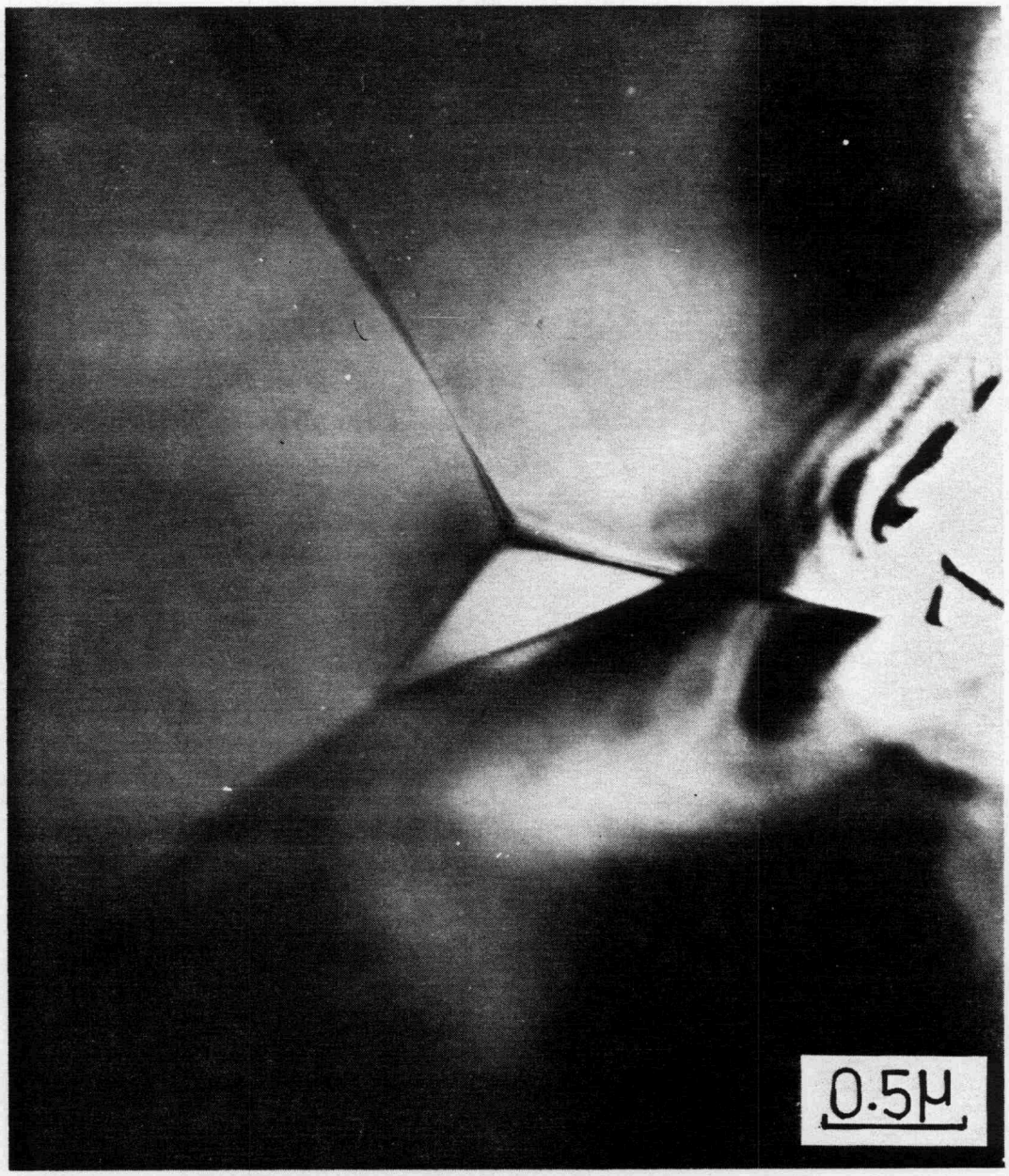

Fig. 13 Scanning transmission electron micrograph of typical intergranular structure for Wesgo AL-995 alumina showing the presence of glassy phase.

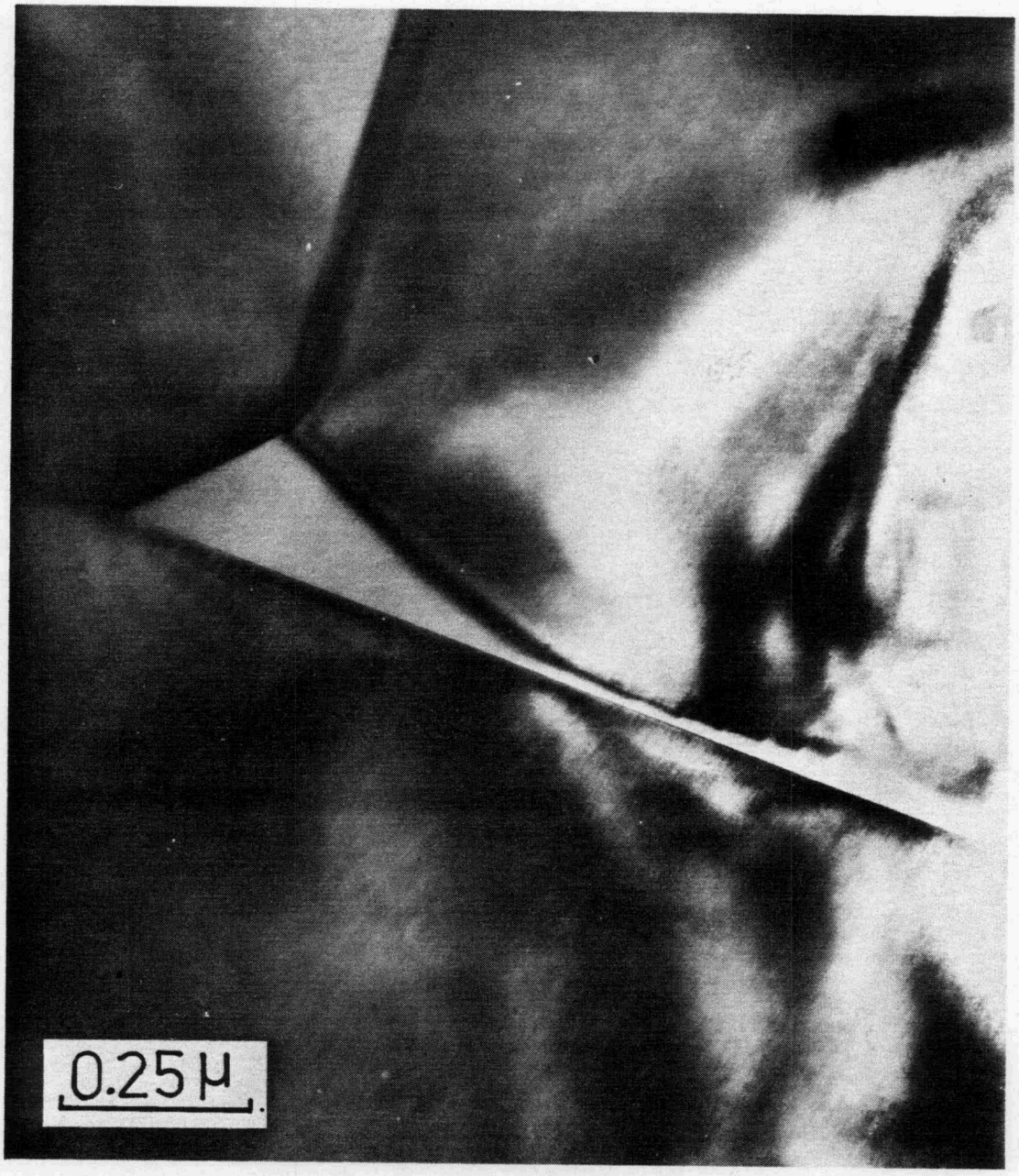

Fig. 14 Scanning transmission electron micrograph of typical intergranular structure for Coors AD-995 (batch 8360, firing No. L58-150) alumina showing the presence of glassy phase.

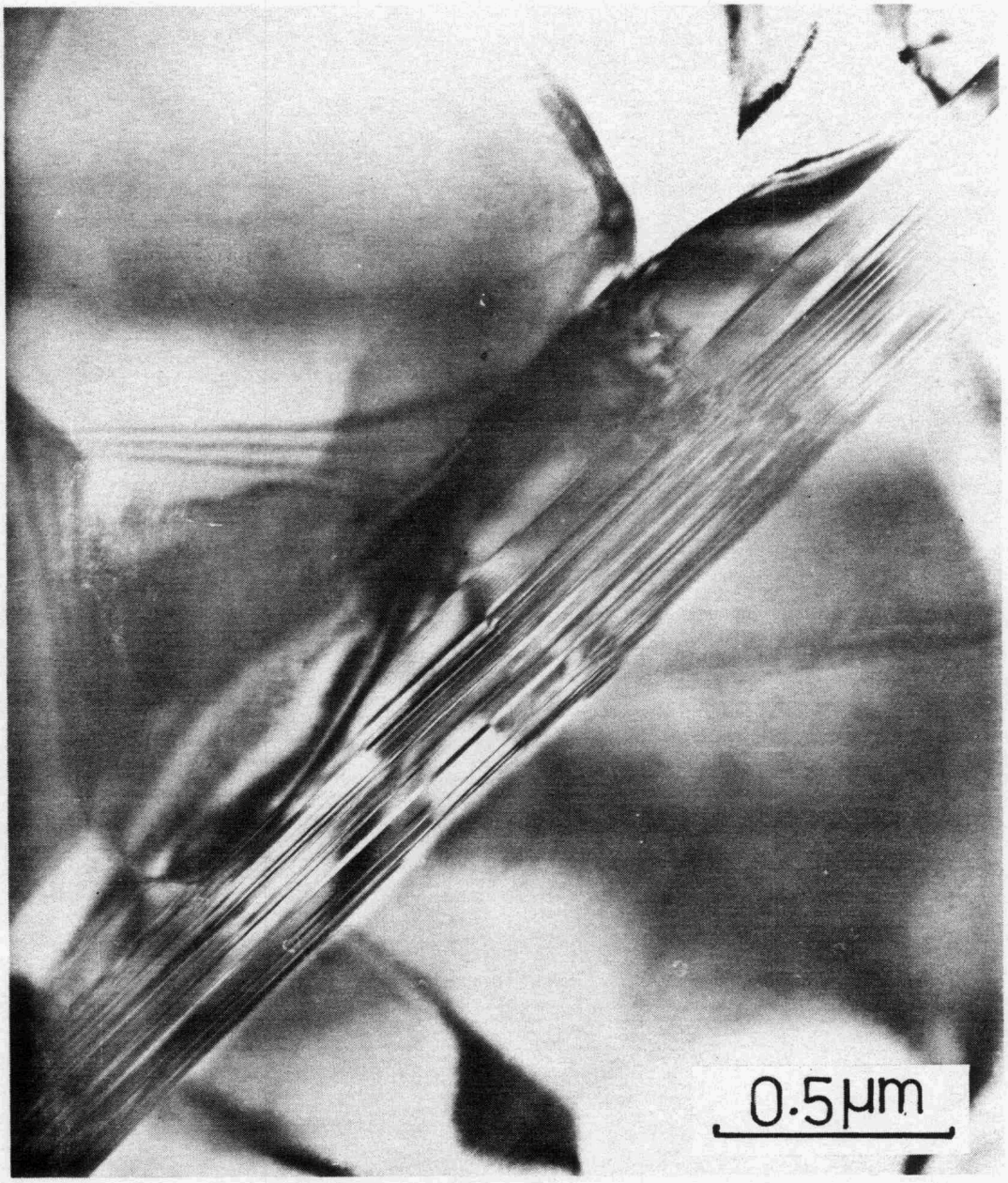

Fig. 15 Scanning transmission electron micrograph of Coors AD-999 alumina sample. Large particles with beta alumina-like structures are present.

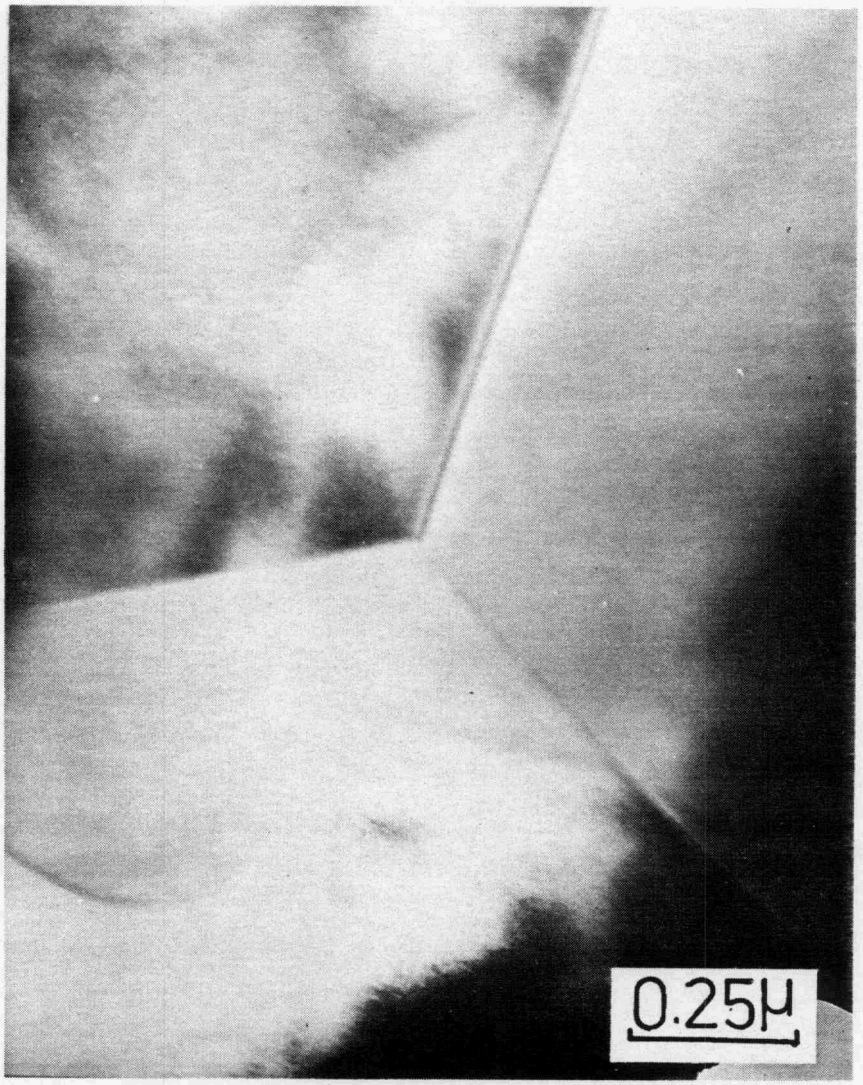

Fig. 16 Scanning transmission electron micrograph of Union Carbide hot-pressed alumina sample (Al_2O_3-CR-10-18) showing the absence of any detectable glassy phase.

WESGO 995 Alumina

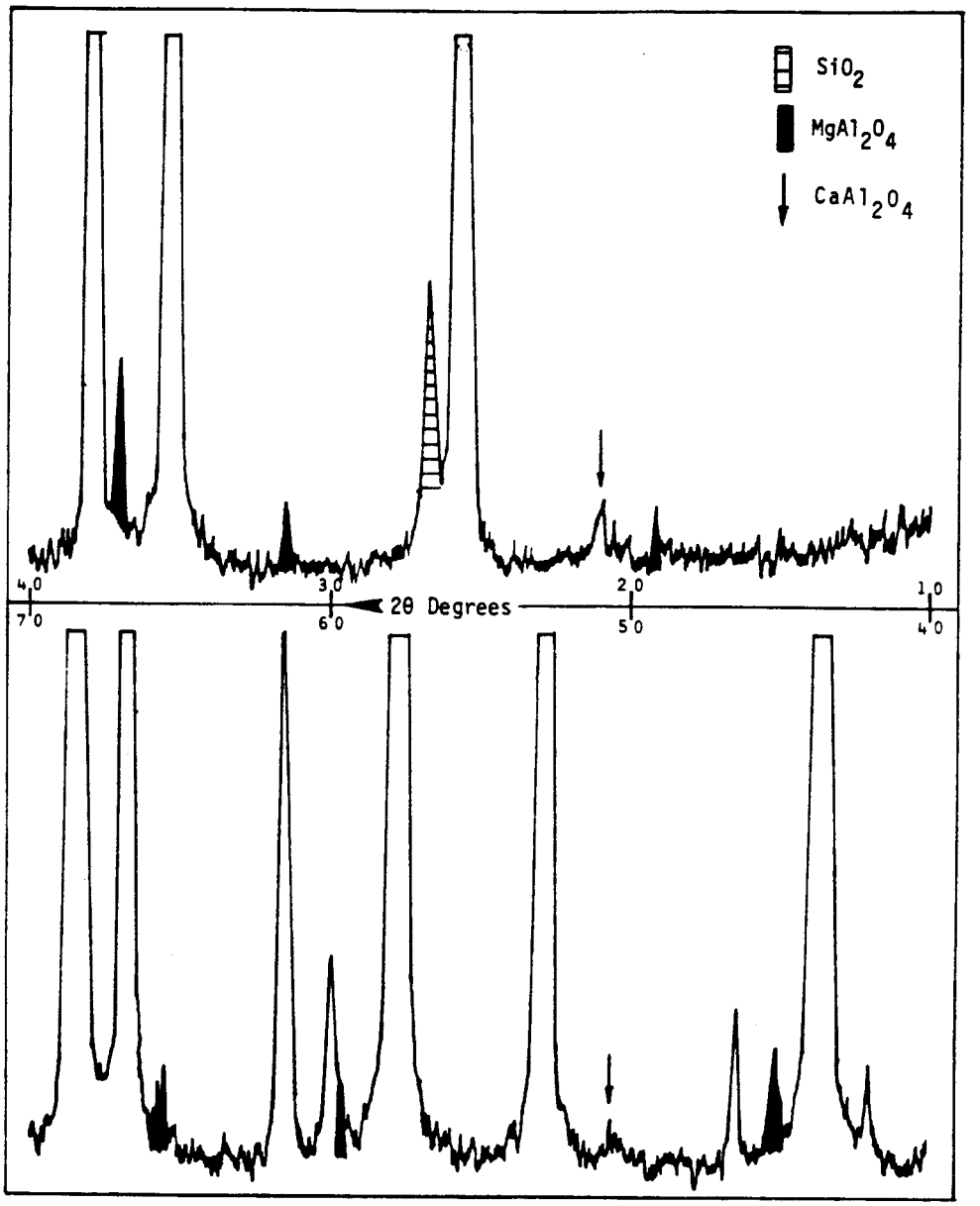

Fig. 17 Powder x-ray diffraction pattern of Wesgo AL-995 alumina sample showing presence of silica, spinel, and calcium aluminate as crystalline secondary phases.

COORS 995 Alumina

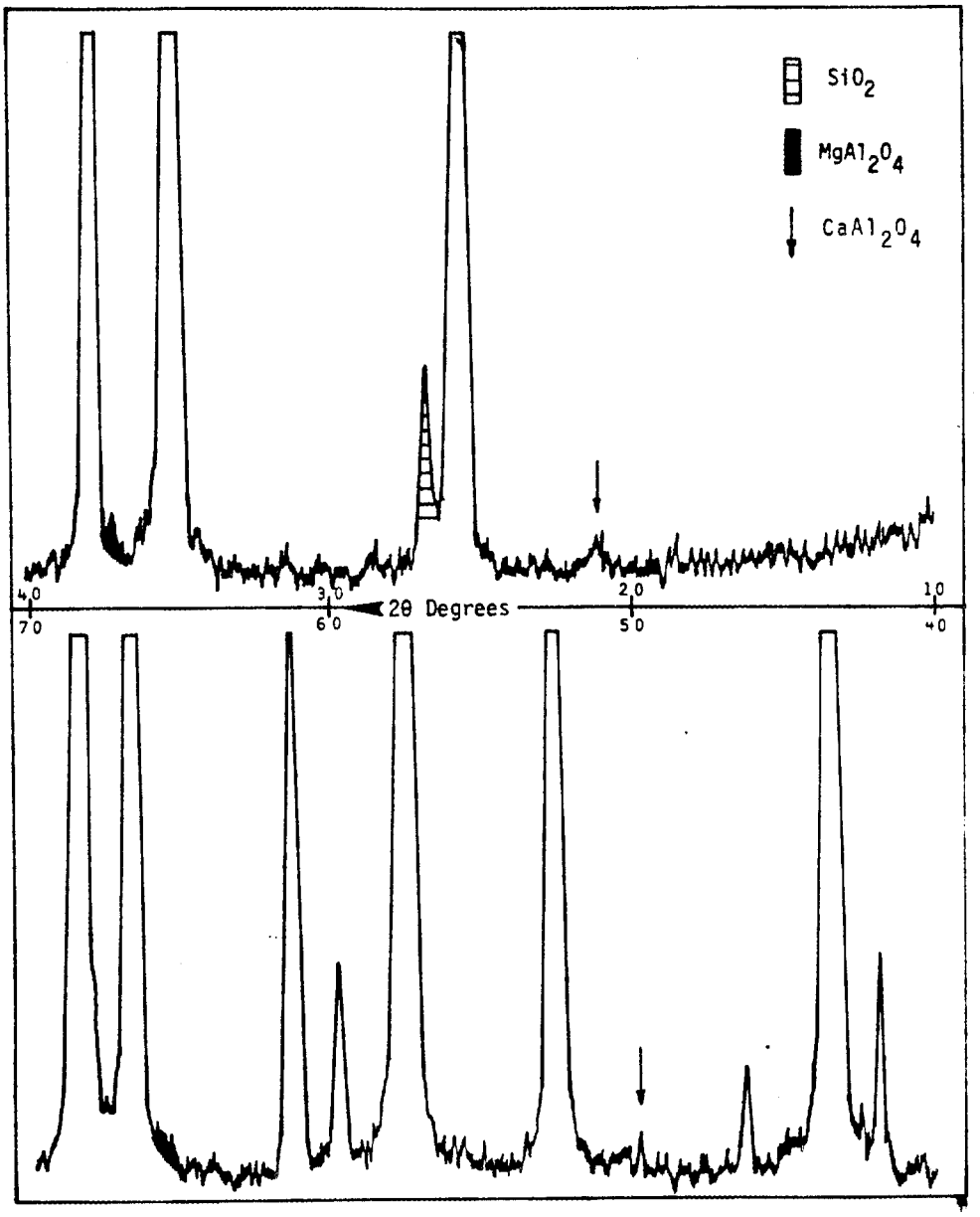

Fig. 18 Powder x-ray diffraction pattern of Coors AD-995 alumina sample. The concentrations of silica, spinel and calcium aluminate are lower by comparison to the Wesgo AL-995 material.

COORS 999 Alumina

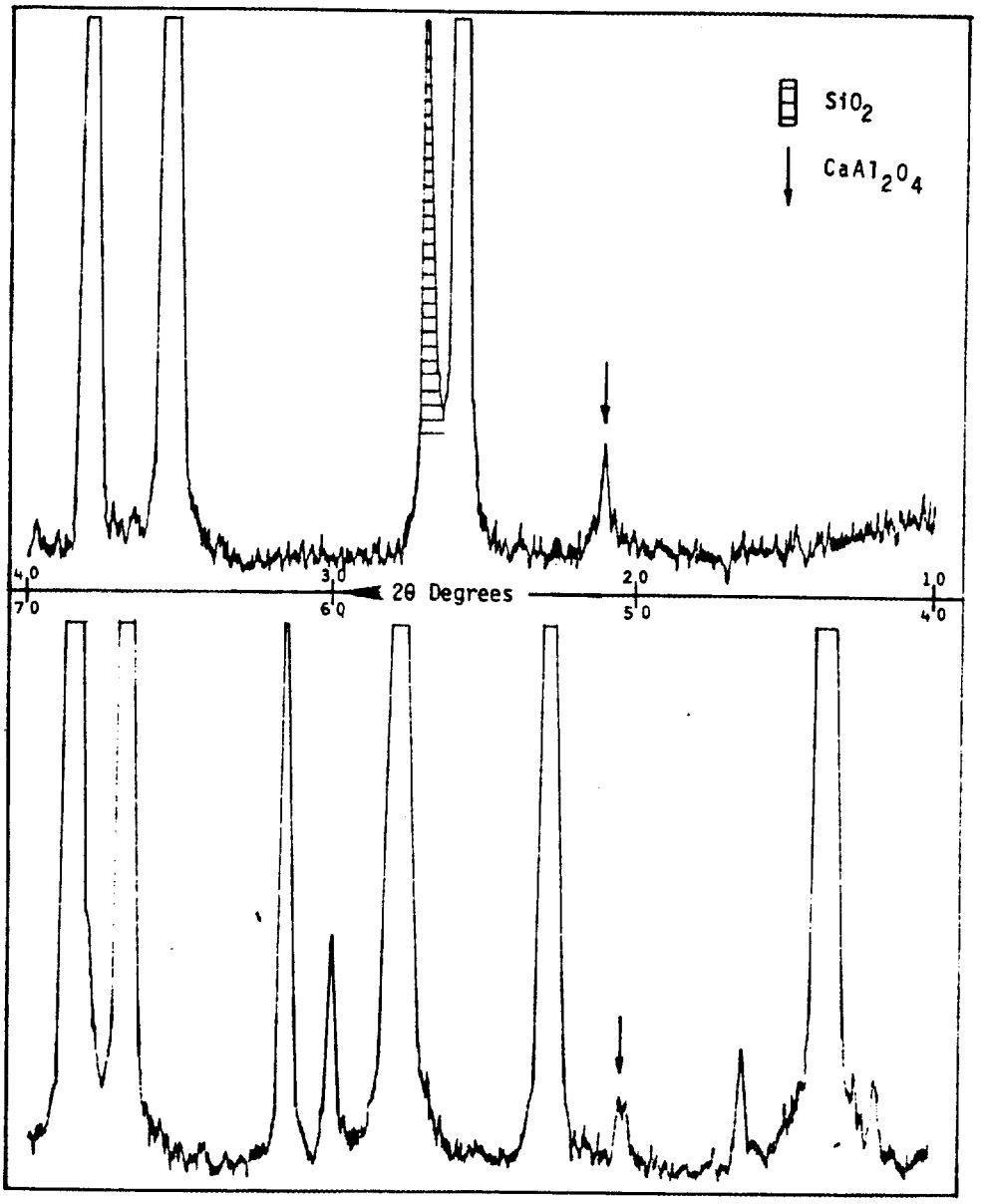

Fig. 19 Powder x-ray diffraction pattern of Coors AD-999 alumina sample. The concentrations of silica and calcium aluminate secondary crystalline phases are much higher, but there is no evidence for the presence of spinel.

UNION CARBIDE Alumina

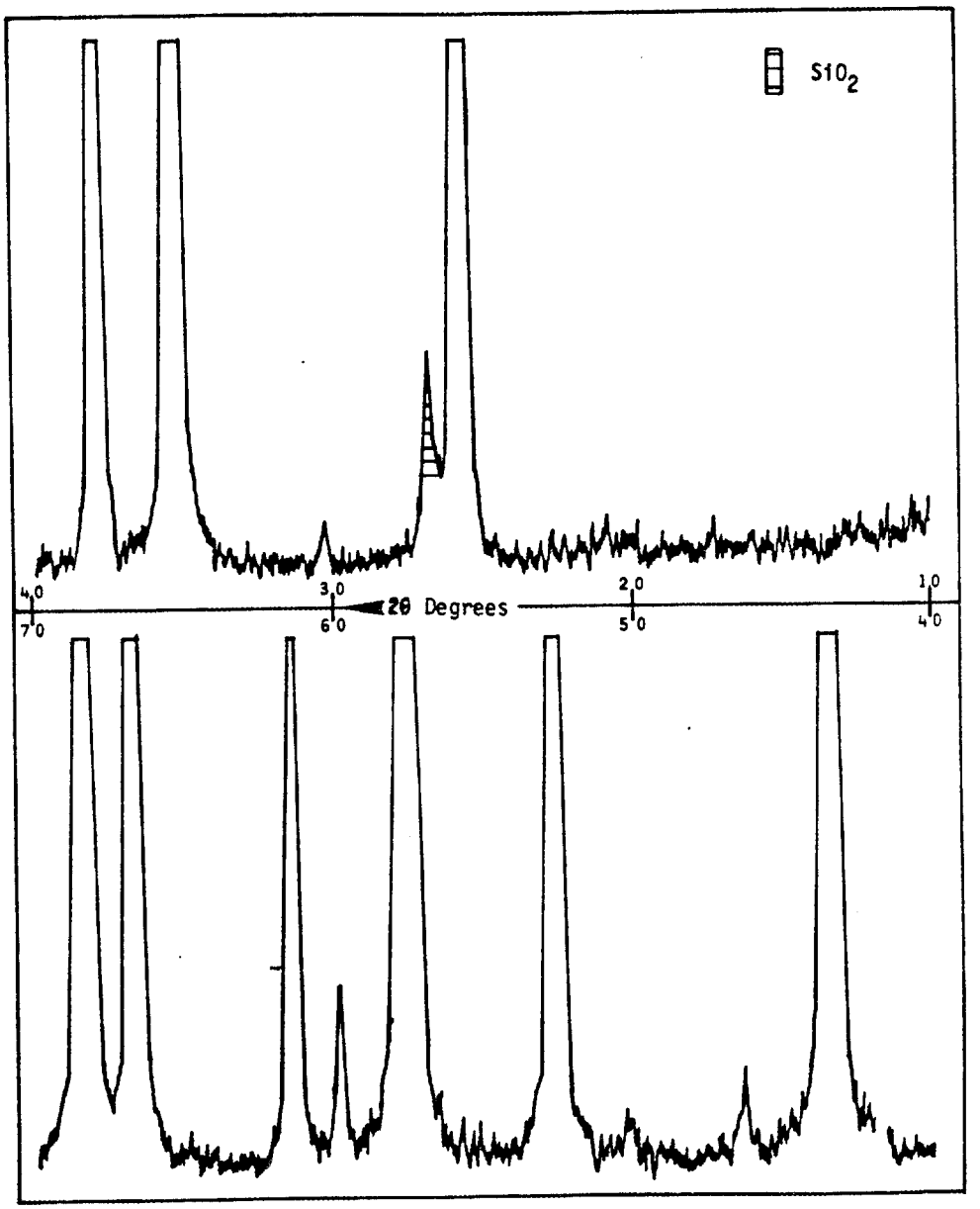

Fig. 20 Powder x-ray pattern of Union Carbide hot-pressed alumina sample, showing no peaks associated with spinel or calcium aluminate and low concentration of silica.

Alumina Powder

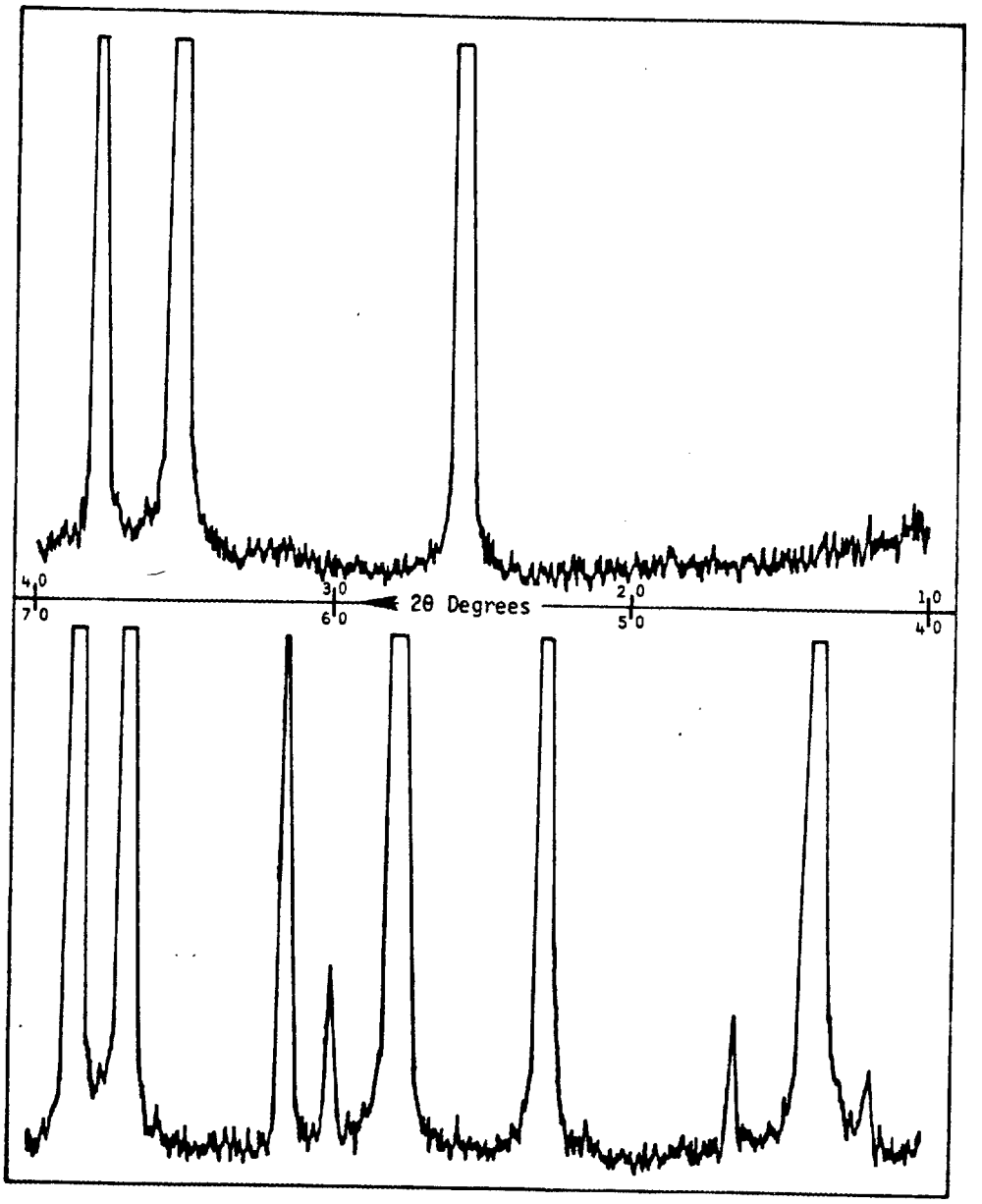

Fig. 21 X-ray diffraction pattern of alumina starting powder used in fabrication of Union Carbide sample. There is no evidence of any peak associated with crystalline phases other than Al_2O_3.

WESGO 995 Alumina

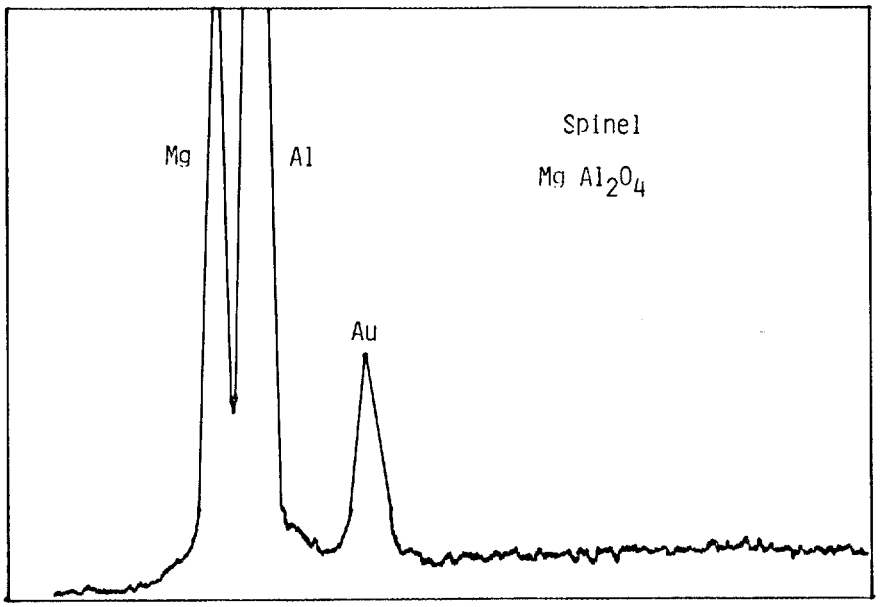

Fig. 22 SEM and EDAX data for crystalline spinel found in the Wesgo AL-995 material.

COORS 995 Alumina

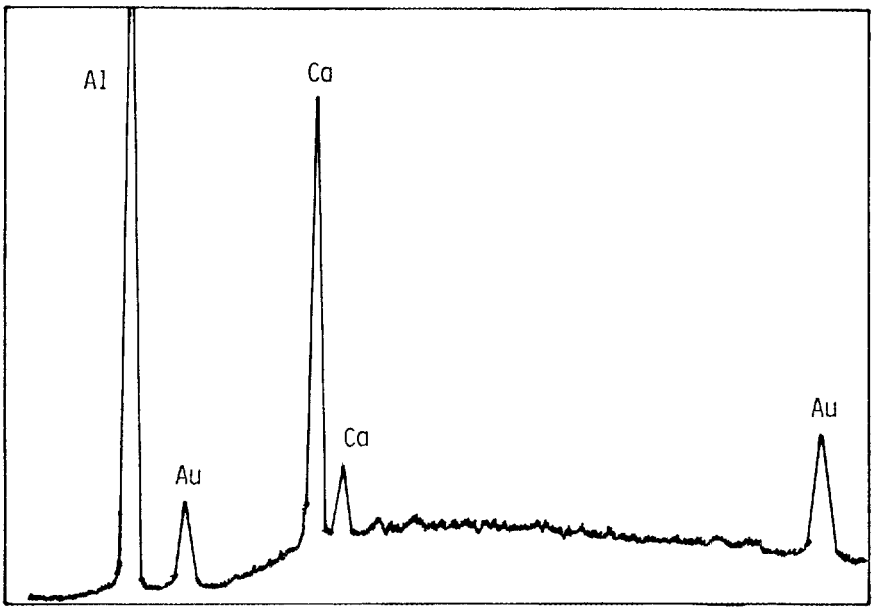

Fig. 23 SEM and EDAX data for crystalline calcium aluminate found in the Coors AD-995 material.

relatively free of silica. The Union Carbide material showed the lowest level of SiO_2 with no evidence of either Ca or Mg secondary crystalline phases.

Although the results obtained from these chemical and microstructural studies of ceramic alumina are preliminary in nature, and further in-depth systematic analysis need to be carried out before the mechanisms controlling the millimeter wave loss properties can be quantified, some tentative observations can be made from the data presented. In general, the measured millimeter wave loss in ceramic alumina is higher than that in single crystal sapphire throughout the frequency range studied. If the data for sapphire is a good indication of the intrinsic loss contribution from the low frequency wing of the infrared lattice transitions for Al_2O_3, then the excess absorptions in ceramic alumina can be attributed to extrinsic loss mechanisms associated with secondary phases and impurities. Since pure secondary phases such as fused silica, spinel, MgO, etc., are very low loss materials, it is not their presence which increases the loss in alumina, but the level of impurities which are incorporated into these crystalline as well as other amorphous intergranular phases which are most probably the main contributors to the extrinsic loss. For instance, the presence of small concentrations of impurities such as Mg, Ca, Na, etc., can increase the millimeter wave loss in fused silica by over an order of magnitude. Consequently, the key parameter in determining loss is not necessarily the total concentration of additives and impurities but depends on their chemical form and their distribution within the material. Hence the occurrence of high concentrations of secondary crystalline phases within an alumina sample (such as those observed in the Coors AD-995 and Wesgo AL-995 samples) will be detrimental to the loss properties only if the cations associated with these secondary phases are also incorporated into other chemical compositions which are absorbing. The distribution of cation additives and impurities will most probably depend on the alumina microstructural properties such as grain size as well as on the physical and chemical properties at the intergranular boundaries.

The materials properties of the Wesgo AL-995 and Coors AD-995 alumina are sufficiently similar in terms of grain size, grain morphology, secondary crystalline phases and intergranular amorphous phases such that the physical and chemical distributions of the cations present are also expected to be similar. Hence the observed differences in dielectric properties can be reasonably attributed to minor differences in the measured materials properties. The higher dielectric constant observed for the Coors AD-995 material is certainly due to lower porosity, while the higher loss for the Wesgo AL-995 material is most probably due to the higher concentrations of impurities present. The primary detected cations for these materials are Si, Mg, Ca and Fe. The STEM and XRD results all showed that their concentrations are higher in the Wesgo material when compared to the Coors Material in both secondary crystalline phases and intergranular phases. We therefore expect that improvement in dielectric loss in this class of alumina can be achieved by further lowering the concentration of these cations.

Although we have seen evidence of contamination which could conceivably explain the observed loss tangent in the Union Carbide hot-pressed alumina sample, the general observation of high loss in the fine grained ceramic alumina sample remains puzzling. While the range of grain sizes observed in the samples studied are all very much smaller than the wavelengths of observations so that there should not be any direct effects on millimeter wave bulk dielectric properties, this size difference could influence the distribution of impurities in such a way as to enhance the loss in the finer grained materials. One possible explanation would be that impurities tend to concentrate at the grain boundaries. Since the intergranular surface area associated with fine grained material is much larger than that for the coarser grained material, the net amount of impurities at the grain surfaces would be larger in the fine grained material even though the total bulk concentration may be much less. These impurities could be in chemical states which have high microwave absorption, or alternatively, could induce defects or changes in surface stoichiometry of the Al_2O_3 grains. The modified surfaces then can

cause a broadening of the infrared lattice transitions for Al_2O_3 thus increasing the absorption in the low frequency wing of the band. If this speculation is correct, it would imply that impurities need to be controlled to a much lower concentration level in fine grained alumina in order to achieve the same loss tangent values as for the larger grained material.

4.2 Single Crystal Sapphire

The Z-cut single crystal sapphire samples used in this study were manufactured by Crystal Systems, Inc. and are disks 7.620 cm in diameter and 0.2261 cm thick. The crystals are oriented such that the measured dielectric properties correspond to the case where the millimeter wave electric field is perpendicular to the crystal axis, (or the lower dielectric constant direction). Four samples were measured, and they showed identical properties. The data obtained are shown in Table III. Since the thickness of each individual sample was not large enough to allow loss determination to be carried out, additional experiments were performed by stacking all four samples together in order to increase the total optical pathlength. The agreement in the measured dielectric constant for the individual samples and with the samples stacked together indicated that effects caused by possible presence of air gaps were negligible. Although the measurement error for the loss tanget is still somewhat large, the data indicated that this material has the best millimeter wave loss characteristics of all of the window candidates examined in this program.

4.3 Other Ceramics

Dielectric measurements were carried out on a plate sample of aluminum oxynitride (ALON) furnished by Raytheon Co., and on several hot pressed samples of ceramic beryllium oxide (BeO) furnished by Union Carbide/Oak Ridge, with the free-space transmission and reflection method between 35 GHz and 110 GHz. In addition, measurements were also carried out on small rod samples of various ceramics using the cavity perturbation technique at 35 GHz.

Table III

Single Crystal Aluminum Oxide (Sapphire) Data Summary

Manufacturer: Crystal Systems, HEMLITE, Standard Optical Grade
Crystal Orientation: Electric Field Perpendicular to Crystal C-Axis
Sample Diameter: 7.620 cm*
Sample Thickness: 0.2261 cm*
Sample Density: 3.979 gm/cc*

	33-50 GHz		50-75 GHz		90-100 GHz	
Sample No.	k	tanδ ($\times 10^{-5}$)	k	tanδ ($\times 10^{-5}$)	k	tanδ ($\times 10^{-5}$)
1 Through 4	9.389 (±0.005)	-	9.387 (±0.050)	-	9.388 (±0.005)	-
All 4 Samples Stacked	9.386 (±0.003)	<20	9.385 (±0.003)	<20	9.385 (±0.003)	25±15

Temperature Dependence Studies at 90-100 GHz
(All 4 Samples Stacked)

Temperature (°C)	k	tanδ
25	9.39	0.00025 ± 0.00015
100	9.42	0.00025 ± 0.00015
200	9.47	0.00025 ± 0.00015

*All 4 samples studied have identical properties.

The ALON sample obtained from Dr. Thomas Hartnett of Raytheon was approximately 10.6 cm in diameter and appeared to be of extremely high optical quality. The BeO samples were hot pressed in the temperature range 1300°C to 1400°C with MgO added as a sintering aid. The three samples, as delivered from Ceradyne Inc., were not identified other than faint pencil marks of 1, 2 and 3 written on the samples. The overall color appearance of the center of the samples ranged from milky white to light tan. The measured dielectric properties for the ALON sample and the BeO samples are summarized in Tables IV and VI, respectively. The ALON material showed a loss comparable to the best alumina at 35-45 GHz, but increases much more rapidly as a function of frequency. Its value is approximately 2.5 larger than alumina in the 90-100 GHz frequency region. For the three BeO samples studied, there are significant differences in both the values of dielectric constant and loss tangents among the samples, with sample No. 3 showing the highest dielectric constant value and lowest loss, and sample No. 2 showing the lowest dielectric constant value

and highest loss. Interestingly enough, sample No. 3 was of the darkest color with significant number of gray spots distributed throughout the sample, while sample No. 2 has the lightest and most uniform appearance. The same rapidly increasing trend in the loss tangent as a function of frequency similar to ALON, is observed for all three samples, while the value at 35-45 GHz in the best sample is again comparable to the other very low loss ceramic materials.

The data obtained for hot-pressed spinel and various different types of silicon nitride ceramics are given in Tables IV, V and VI. The sintered silicon nitride samples furnished by Dr. Charles D. Greskovich of General Electric are doped with oxygen and beryllium (~ 1%) and have been oxidized at 1355°C and 1415°C for several hundred hours. The GTE AY6 and PY6 silicon nitride samples were sintered with 6% Y_2O_3 with 2% Al_2O_3 added in the AY6 material. These samples were further heat-treated at approximately 1300°C in oxygen for 100 h to reduce the concentration of cations in the integranular amorphous glassy phase. The measured dielectric properties are shown in Tables V and VI, while the temperature dependence of the loss tangents in the GTE AY6 and PY6 materials are given in Fig. 24. Both GE and GTE sintered silicon nitride materials have dielectric constants somewhat smaller than typical commercial hot-pressed materials. The loss tangents are approximately a factor of two lower than typical values in commercial hot-pressed silicon nitride, but are still an order of magnitude higher than those observed in silicon nitride fabricated by chemical vapor deposition processes.

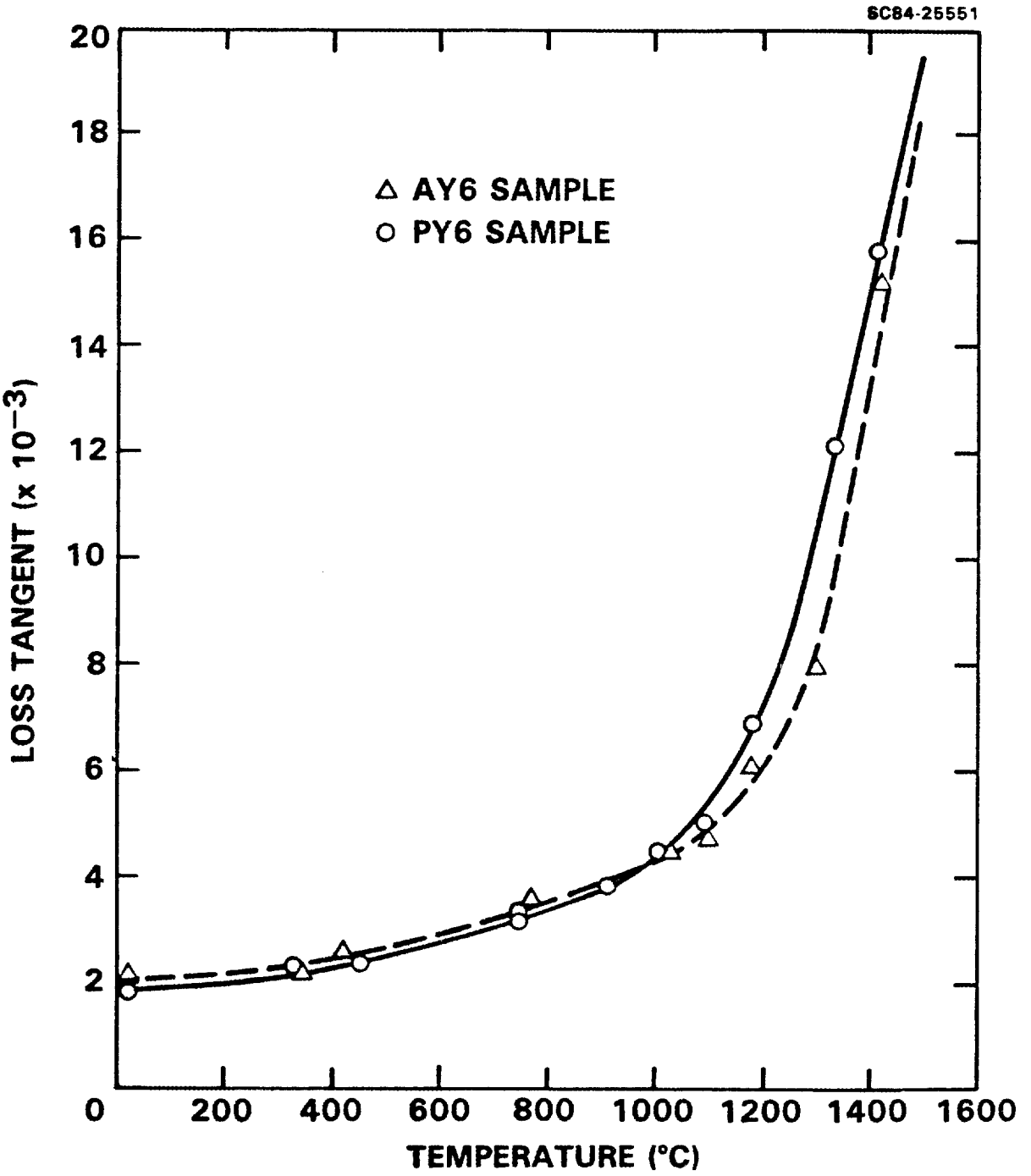

Fig. 24 Measured loss tangents as a function of temperature for GTE AY6 and PY6 sintered silicon nitride at 35 GHz.

Table IV

Hot-pressed Ceramic Spinel ($MgOAl_2O_3$) Data Summary

Manufacturer: Furnished by Raytheon
Sample Shape: Thin rod, 0.0602 cm diameter
Measurement Method: Cavity perturbation
Frequency: 35 GHz

Temperature (°C)	k (±0.03)	tanδ ($x10^{-5}$) (±15)
25	8.35	23
490	9.03	38
740	9.45	60
900	9.73	82
1020	9.94	104
1100	10.20	183
1180	10.44	312

Aluminum Oxynitride (ALON) Data Summary

Manufacturer: Raytheon (high optical quality)
Sample Diameter: 10.6 cm
Sample Thickness: 0.373 cm
Sample Density: 3.68 gm/cc

35-45 GHz		55-60 GHz		90-110 GHz	
k	tanδ($x10^{-5}$)	k	tanδ($x10^{-5}$)	k	tanδ($x10^{-5}$)
9.190 (±0.005)	31 ± 15	9.181 (±0.005)	67 ± 15	9.175 (±0.008)	96 ± 15

Table V

Sintered Silicon Nitride (Si_3N_4) Data Summary

Manufacturer: GTE Laboratories, Inc.
Sample Type: AY6 (Si_3N_4/6 w/o Y_2O_3/2 w/o Al_2O_3)
PY6 (Si_3N_4/6 w/o Y_2O_3)
Measurement Method: Cavity perturbation
Frequency: 35 GHz

Room Temperature Properties (23°C)		
Temperature (°C)	k (±0.05)	tanδ ($\times 10^{-4}$) (±10)
AY6	7.98	23
	7.91	22
PY6	7.74	31
	7.68	19

Temperature Studies		
Temperature (°C)	PY6 k_t/k_r	AY6 k_t/k_r
440	1.025	1.040
765	1.055	1.074
916	1.070	1.099
1035	1.082	1.105
1100	1.090	1.120
1180	1.104	1.130

Table VI

Room Temperature (23°C) Dielectric Properties at 35 GHz for Sintered Si_3N_4 (1% BeO)

Material	k (±0.10)	tanδ ($x10^{-4}$)
G.E. Sintered Si_3N_4		
1. Oxidized at 1355°C for 213 hours	7.35	22 ± 5
2. Oxidized at 1415°C for 280 hours	7.62	17 ± 5

Hot-pressed Beryllium Oxide (BeO) Data Summary

Manufacturer: Union Carbide (obtained through Ceradyne Inc.)
Sample Type: Hot-pressed with MgO added at 1300°C, 1350°C and 1400°C

		35-45 GHz		55-60 GHz		90-110 GHz	
Sample No.	Thickness (cm)	k (±0.01)	tanδ($x10^{-5}$)	k (±0.01)	tanδ($x10^{-5}$)	k (±0.02)	tanδ($x10^{-5}$)
1	1.834	6.62	54 ± 15	6.62	82 ± 15	6.61	106 ± 15
2	1.834	6.43	90 ± 15	6.42	112 ± 15	6.41	135 ± 15
3	1.819	6.78	28 ± 15	6.78	45 ± 15	6.77	75 ± 15

The data obtained for hot-pressed spinel at 35 GHz as a function of temperature are given in Table IV. The room temperature loss tangent is lower than the best ceramic alumina and comparable to the measured values in single crystal sapphire. The general behavior of the dielectric properties as a function of temperature is similar to that observed for alumina as given in Table II, except that the rate of increase is somewhat faster. Since the frequency dependence of the loss tangent for this material was shown by Afsar and Button to be very similar to alumina in the 100-400 GHz frequency range, (M.N. Afsar and K.J. Button, "Digest of mm and Sub-mm Wave Materials Information and Measurements," FBMNL, MIT, Cambridge, MA, 1983) its losses are

not expected to increase drastically as a function of frequency. Consequently, in contrast to the behavior found for ALON and BeO, the loss in this material should compare favorably with alumina throughout the entire millimeter frequency region.

4.4 Fluorocarbon Fluids

Three different types of nonpolar fluorocarbon fluids were studied. They are manufactured by the Commercial Chemical Division of the 3M Corporation and are identified under the trade names Fluorinert FC-43, FC-75 and FC-104. Measurements were carried out on samples taken directly from sealed containers as delivered from the manufacturer to minimize contamination. The samples are loaded into small quartz capillary tubes and the cavity perturbation method was used to determine their dielectric properties at 8.36 GHz, 35 GHz, 60 GHz and 95 GHz. Calibration runs were performed for all cases on empty sample tubes and on the tubes filled with a known standard liquid (CCl_4).

The data shown in Table VII indicated that the FC-75 and FC-104 samples are very similar in their dielectric response, with FC-75 showing slightly less loss. By contrast the FC-43 fluid has a larger dielectric constant and significantly less loss at the higher frequencies. Exposure of FC-75 fluid to liquid water increased the observed loss at 8 GHz slightly, but did not affect the loss at millimeter wave frequencies. A slight decrease in dielectric constant was observed for FC-75 over the temperature range 23-50°C, which is most probably due to density changes. The loss tangent, however, remained virtually the same as its room temperature value.

Table VII
Fluorocarbon Fluid (Flouroinert) Data Summary
Manufacturer: 3M Company

Room Temperature Dielectric Properties (23°C)								
	8.36 GHz		35 GHz		60 GHz		95 GHz	
Sample Type	k (±0.005)	tanδ (±0.0005)	k (±0.005)	tanδ (±0.05)	k (±0.01)	tanδ (±0.001)	k (±0.02)	tanδ (±0.001)
FC-43 (98-0204-1103-3)	1.854	0.0069	1.850	0.0045	1.86	0.003	1.86	0.001
FC-75 (98-0204-0303-0)	1.794	0.0075	1.781	0.0051	1.78	0.004	1.78	0.003
FC-104 (98-0204-0103-4)	1.779	0.0083	1.767	0.0066	1.77	0.005	1.77	0.004
FC75 + H_2O (72 hr exposure to liquid water)	1.793	0.0083	1.783	0.0053	1.78	0.004	1.78	0.003

Temperature Dependence Studies for FC-75 at 35 GHz		
Temperature	k	tanδ
23°C	1.781	0.0051
30°C	1.763	0.0050
40°C	1.749	0.0049
50°C	1.735	0.0050

5.0 CONCLUSIONS AND RECOMMENDATIONS

The results obtained for the millimeter wave dielectric properties of the Al_2O_3 materials studied in this program indicated that, as expected, single crystal sapphire has the lowest loss tangent. The best ceramic alumina samples (Coors AD-995, Ampex 99.5%, Wesgo AL-995) have losses approximately a factor of 2 larger at 90-100 GHz, while the fine grained alumina samples (Coors AD-999, Union Carbide hot-pressed alumina) showed surprisingly high losses when compared to sapphire. Preliminary chemical and microstructural analysis carried out on these ceramic samples yielded noticeable differences in trace element composition, grain structure, and secondary and intergranular phases. Establishment of the correlation of these material properties with the observed dielectric response is essential in order to provide the necessary information for developing advanced ceramic alumina materials with properties approaching those for sapphire. Further research towards this goal is strongly recommended.

In addition, it is not clear at present whether the measured loss tangent in sapphire is intrinsic to the material or still dominated by trace impurities or crystal defects. To address this issue, accuracy needs to be further improved for the millimeter wave measurements and sample purity needs to be determined and controlled. It is recommended that a systematic study be carried out with well-characterized materials over as wide a frequency range as possible so that the dielectric response can be accurately determined. Improvement in the measurement accuracy can be obtained by using thicker samples, and dielectric measurements need to be carried out for both crystal orientations.

Of the other candidate ceramic materials examined, hot-pressed spinel was found to have loss tangents comparable to sapphire and better than the best alumina material. The various silicon nitride samples all showed loss tangents which are significantly higher, and it is likely that extensive materials development efforts need to be undertaken before they can be

significantly improved to be comparable to alumina or sapphire. ALON and BeO have loss tangents comparable to the best alumina material at 35 GHz, but are substantially higher than alumina at 90-110 GHz.

The fluorocarbon fluids all showed a decreasing trend in loss tangent values with increasing frequency over the range 8.6 to 95 GHz, implying the presence of a low-frequency dispersion peak. The observed faster fall-off in the millimeter wave region for the FC-43 fluid may be due to the fact that this dispersion is occurring at a lower frequency than those for the FC-75 and FC-104 fluids. It would be desirable to have data available in the frequency range below 8 GHz so that loss mechanism in this class of liquids can be better understood.

INTERNAL DISTRIBUTION

1. P. F. Becher
2. T. S. Bigelow
3. M. K. Ferber
4. H. H. Haselton
5. H. D. Kimrey, Jr.
6. R. P. Jernigan
7-9. C. M. Loring, Jr.
10. H. C. McCurdy
11. D. H. Metzler
12. O. B. Morgan, Jr.
13. J. L. Scott
14. J. M. Spicer, ORNL Patent Office
15. T. L. White
16. F. W. Wiffen
17-18. Laboratory Records Department
19. Laboratory Records, ORNL-RC
20. Y-12 Document Reference Section
21-22. Central Research Library
23. Fusion Energy Division Library
24. Fusion Energy Division Communications Center

EXTERNAL DISTRIBUTION

25. D. S. Beard, Component Branch, Office of Fusion Energy (ETM), Department of Energy, ER-531, GTN, Washington, DC 20545
26. H. Bennett, Code 38101, U. S. Naval Weapons Center, China Lake, CA 93555
27. K. J. Button, Francis Bitter Nat'l Laboratory, MIT, Cambridge, MA 02139
28. R. A. Dandl, 1122 Calle De Los Serranos, San Marcos, CA 92069
29. R. J. DeBellis, McDonnell Douglas Astronautics Co., P. O. Box 516, St. Louis, MO 63166
30. J. F. Decker, Office of Fusion Energy, Dept. of Energy, APP, Rm. 219, ER-54, GTN, Washington, D. C. 20545
31. N. Dionne, Raytheon Company, Foundry Avenue Waltham, MA 02254
32. W. P. Ernst, Princeton University, Plasma Physics Laboratory, P. O. Box 451, Princeton, NJ 08540
33. D. Evans, AFAL/MLPO Wright-Patterson AFB, OH 45433
34. P. Ferguson, 2402 Thaddeus Drive, Mt. View, CA 94043
35. J. D. Fowler, Los Alamos Nat'l Laboratory, MS-546, Los Alamos, NM 87545
36. J. Fuller, Eng'g Experiment Station, Ga. Institute of Tech., Atlanta, GA 30332
37. T. V. George, Office of Fusion Energy (ETM), Department of Energy, 19901 Germantown Road, Germantown, MD 20767
38. T. Godlove, Particle Beam Program, Office of Inertial Fusion, Department of Energy, Mail Stop C-404, Washington, DC 20545
39. V. L. Granatstein, University of Maryland, College Park, MD 20742
40. C. Greskovich, General Electric Co., Corporate R&D, Schenectady, NY 12301

41. G. M. Haas, Component Development Branch, Office of Fusion Energy (ETM), Department of Energy, ER-531, GTN, Washington, DC 20545

42. M. Haas, Naval Research Laboratory, Washington, DC 20545

43. G. W. Hamilton, Reactor Design, MFE Program, Lawrence Livermore National, L6-44, P. O. Box 5511, Livermore, CA 94550

44. T. M. Hartnett, Raytheon Res. Div., 131 Spring St., Lexington, MA 02173

45. J. L. Hirshfield, Yale University, Department of Engineering and Applied Science, P. O. Box 2159, Yale Station, New Haven, CT 06550

46. D. B. Hopkins, Lawrence/Berkeley Laboratory, Bldg. 46 S., Berkeley, CA 94720

47. H. R. Jory, Varian Associates, 611 Hansen Way, MS-B109, Palo Alto, CA 94303

48. R. N. Katz, Ceramic Research Division, Army Materials and Mechanics Research Center, Arsenal Street, Watertown, MA 02172

49. K. Krause, Lawrence Livermore National Laboratory, P. O. Box 808/L-634, Livermore, CA 94550

50. J. V. Lebacqz, Stanford Linear Accelerator Center, P. O. Box 4349, Bin 30, Stanford, CA 94305

51. W. Lindquist, Electronics Engineering Department, Lawrence Livermore Laboratory, P. O. Box 808/L-443, Livermore, CA 94550

52. W. T. Messick, Naval Surface Weapons Center, White Oak Laboratory, Silver Springs, MD 20910

53. H. Mizuhara, GTE/Wesgo, 477 Harbor Boulevard, Belmont, CA 94002

54. C. Moeller, General Atomic Company, P. O. Box 81608, San Diego, CA 92138

55. J. H. Pfannmuller, McDonnell Douglas Astronautics Co., C/O Oak Ridge National Laboratory, P. O. Box Y, FEDC Building, Oak Ridge, TN 37830

56. G. F. Pierce, 53 Lomond Drive, Inverness, IL 60067

57. R. Pohanka, ONR, Code 471, 800 N. Quincey, Arlington, VA 22217

58. R. Prater, Doublet III ECH Program, General Atomic Company, P. O. Box 81608, San Diego, CA 92138

59. C. L. Quackenbush, GTE Laboratories, Inc., 40 Sylvan Rd., Waltham, MA 02254

60. B. H. Quon, TRW Defense & Space Systems, 1 Space Park, Bldg. R-1, Redondo Beach, CA 90278

61. M. E. Read, Naval Research Laboratory, Code 6740, Washington, DC 20375

62. R. Rice, Naval Research Laboratory, Code 6360, Washington, DC 20375

63. T. Roemesser, TRW Defense & Space Systems, 1 Space Park, Building R-1, Redondo Beach, CA 90278

64. F. Schmid, Crystal Systems Inc., 35 Congress Street, Salem, MA 01970

65. G. Simonis, Harry Diamond Laboratory, 2800 Powder Mill Rd., Adelphi, MD 20783

66. M. S. Sparks, Scientific Res. Center, 9507 High Ridge Place, Beverly Hills, CA 90210

67. B. Stallard, Lawrence Livermore Laboratory, University of California, L-437, P. O. Box 808, Livermore, CA 94550

68. H. S. Staten, Office of Fusion Energy (ETM), Department of Energy, ER-531, GTN, Washington, DC 20545
69. M. A. Stroscio, AFOSR, Bolling Air Force Base, Washington, DC 20332
70. P. J. Tallerico, AT-5, Accelerator Technology Division, Los Alamos Scientific Laboratory, Mail Stop H827, P. O. Box 1663, Los Alamos, NM 87545
71. J. J. Tancredi, Electron Dynamics Division, Hughes Aircraft Company, 3100 W. Lomita Boulevard, Torrance, CA 90509
72. R. J. Temkin, National Magnet Laboratory, Massachusetts Institute of Technology, 170 Albany St., NW16-254, Cambridge, MA 02139
73. D. Wirth, Coors Porcelain Company, R&D, Golden, Colorado 80401
74. R. Zacharias, AFAL/DHM, Wright-Patterson AFB, OH 45433
75. Director, U. S. Army Ballistic Missle Defense Advance Technology Center, Attn: D. Schenk, ATC-R, P. O. Box 1500, Huntsville, AL 35807
76. Department of Energy Technical Information Center, Oak Ridge, TN 37830
77. RADC/OCTP, Griffiss AFB, NY 13441
78. Office of Assistant Manager for Energy Research and Development, Oak Ridge Operations Office, Department of Energy, Oak Ridge, TN 37830